NASA CONTRACTOR REPORT

NASA CR-2263

NASA CR-2263

THE RADIATION FROM APERTURES IN CURVED SURFACES

by P. H. Pathak and R. G. Kouyoumjian

Prepared by
THE OHIO STATE UNIVERSITY
ELECTROSCIENCE LABORATORY
Columbus, Ohio 43212
for Langley Research Center

NATIONAL AERONAUTICS AND SPACE ADMINISTRATION • WASHINGTON, D. C. • JULY 1973

1. Report No. NASA CR-2263	2. Government Accession No.	3. Recipient's Catalog No.
4. Title and Subtitle THE RADIATION FROM APERTURES IN CURVED SURFACES		5. Report Date July 1973 6. Performing Organization Code
7. Author(s) P. H. Pathak and R. G. Kouyoumjian		8. Performing Organization Report No. 10. Work Unit No.
9. Performing Organization Name and Address The Ohio State University ElectroScience Laboratory Columbus, Ohio 43212		11. Contract or Grant No. NGR 36-008-144 13. Type of Report and Period Covered Contractor
12. Sponsoring Agency Name and Address National Aeronautics and Space Administration Washington, D.C. 20546		14. Sponsoring Agency Code

15. Supplementary Notes

16. Abstract

In this report the geometrical theory of diffraction is extended to treat the radiation from apertures or slots in convex, perfectly-conducting surfaces. It is assumed that the tangential electric field in the aperture is known so that an equivalent, infinitesimal source can be defined at each point in the aperture. Surface rays emanate from this source which is a caustic of the of the ray system. A launching coefficient is introduced to describe the excitation of the surface ray modes. If the field radiated from the surface is desired, the ordinary diffraction coefficients are used to determine the field of the rays shed tangentially from the surface rays. The field of the surface ray modes is not the field on the surface; hence if the mutual coupling between slots is of interest, a second coefficient related to the launching coefficient must be employed. In the region adjacent to the shadow boundary, the component of the field directly radiated from the source is represented by Fock-type functions. In the illuminated region the incident radiation from the source (this does not include the diffracted field components) is treated by geometrical optics. This extension of the geometrical theory of diffraction is applied to calculate the radiation from slots on elliptic cylinders, spheres and spheroids.

17. Key Words (Suggested by Author(s))	18. Distribution Statement
Aircraft antennas, diffraction theory analysis, computerized antenna design.	Unclassified

19. Security Classif. (of this report)	20. Security Classif. (of this page)	21. No. of Pages	22. Price*
Unclassified	Unclassified	79	$3.00

*For sale by the National Technical Information Service, Springfield, Virginia 22151

TABLE OF CONTENTS

I. INTRODUCTION

The radiation from slots and slot arrays in smooth, curved surfaces is pertinent to the design of flush-mounted antennas for high-speed aircraft and spacecraft. In this report the geometrical theory of diffraction (referred to simply as the GTD henceforth) is extended to treat the radiation from apertures in convex, perfectly-conducting surfaces. The GTD was introduced by Keller[1] as a systematic extension of classical geometrical optics to describe the diffraction phenomenon in terms of rays. Diffracted rays, similar to the ordinary rays of geometrical optics, are introduced to describe the propagation of the diffracted field; these diffracted rays are determined by an extension of Fermat's principle. Within the shadow region the geometrical optics fields are zero, and the diffracted rays alone account for the field. Diffracted rays are produced whenever an incident ray strikes a smooth surface at grazing incidence, or strikes an edge, corner, or a tip of a scattering object. At sufficiently high frequencies the excitation of the diffracted field is a local phenomenon; the diffracted field is related to the incident field by one or more diffraction coefficients, which are functions of the boundary conditions and the local geometry at the point of diffraction. Conservation of power in a strip of rays on the surface is employed to deduce the behavior of the surface ray field; this introduces attenuation constants as parameters. Expressions for the diffraction coefficients and attenuation constants are found from asymptotic high frequency solutions to pertinent canonical problems or by boundary layer techniques. Away from the diffracting surface the behavior of the diffracted field along its ray path is the same as that of the geometrical optics field. The GTD is a high frequency approximation, which is asymptotic in the sense that the accuracy of the approximation generally improves as the frequency increases.

Surface diffracted rays are also produced by apertures or slots in smooth curved surfaces; however, the excitation of these surface diffracted rays cannot be described by the curved surface diffraction coefficients alone as we do for the problem of scattering by a smooth, curved surface. It is therefore necessary to extend the GTD technique to treat the excitation of surface diffracted rays by apertures; we have achieved this extension by introducing launching coefficients which relate the excitation of the surface diffracted rays to the aperture distribution. If the field radiated from the surface is desired, the ordinary curved surface diffraction coefficients are used to determine the field of the rays shed tangentially from the surface rays; this field accounts for the radiation field in the shadow zone of the slot (aperture) in a smooth curved surface. In the region adjacent to the shadow boundary (which divides the region of space surrounding the antenna geometry into the illuminated region and the shadow region), the component of the field directly radiated from the source is represented by Fock-type functions. In the illuminated region the incident radiation from the source (this does not include the diffracted field components which may be present if the curved surface is closed) is treated by

geometrical optics. Usually, these solutions blend smoothly so that a continuous total field is obtained in the entire region of space surrounding the curved surface.

Our reason for using the GTD method stems from the significant advantages to be gained; namely

a) it is simple to use, and yields accurate results;
b) it provides some physical insight into the radiation and scattering mechanisms involved;
c) it can be used to treat problems for which exact analytical solutions are not available; and
d) it can be extended in a straightforward manner to treat the mutual coupling between apertures.

The extension mentioned in d) is achieved by introducing an attachment coefficient (related to the launching coefficient) which converts the field of the surface diffracted rays to the surface current (the field associated with the surface diffracted rays is not the field on the surface). This extension will be the subject of a later report. Even though the GTD is valid for high frequencies, it is surprisingly accurate in a number of cases for lower frequencies; the latter is shown to be true for some of the examples presented in this report. Also we note that as a ray optical technique the GTD is consistent with the reciprocity principle for electromagnetic fields.

Sensiper[2] and Wait[3] have given asymptotic high frequency solutions for the radiation from slots in conducting circular cylinders. Belkina and Weinstein[4] have obtained asymptotic high frequency results for the radiation from slots in conducting spheres. However, none of these earlier results[2,3,4] were cast into the GTD form, and hence their solutions could not be directly extended to treat the radiation from slots in arbitrary convex conducting surfaces. One could use Fock theory and reciprocity to find the radiation field of apertures[5]; however, this method cannot be extended to determine the mutual coupling between apertures. Furthermore, the results given in [5] are not as accurate as the ones presented here. Balanis and Peters[6] have analyzed the radiation from slots in conducting cylinders by using the GTD; their approach is different from ours and is based on an approximate combination of wedge diffraction theory and surface ray theory. However, their results do not yield a continuous pattern across the shadow boundary unless they include higher order multiple diffraction between edges. Even with this included, the pattern still has some error near the shadow boundary, although it is continuous.

Section II describes our extension of the GTD to analyze the radiation from apertures in arbitrary convex conducting surfaces. Expressions for the parameters and special functions involved are given in Section III. Applications of the theory to treat the radiation from slots in elliptic cylinders, spheres and spheroids are presented in

Section IV, where the numerical results obtained are compared with calculations based on rigorous solutions and with measurements.

II. THE GTD FORMULATION

The following development, based on the GTD, is heuristic. Physical arguments are used; ray trajectories are deduced from a generalized Fermat's principle, the variation of the field amplitude along a ray path is found from power conservation in a tube (or strip) of rays, and the diffraction and excitation of waves are treated as local phenomena. The validity of the GTD has been established through its application to a wide variety of antenna and scattering problems, and its present application is tested on certain canonical problems, which also yield the unknown parameters of the GTD solution.

Consider the radiation from a slot or aperture in a curved, perfectly-conducting surface where the external medium is free space. The electric field at a point Q' in the aperture is $\bar{E}(Q')$; it is assumed that the tangential component of this field is known. The magnetic surface current associated with the aperture electric field is

$$\bar{K}_s(Q') = \bar{E}(Q') \times \hat{n}' \tag{1}$$

in which $\hat{n}'$ is the outward directed unit normal vector to the aperture surface at Q'. The infinitesimal magnetic current moment

$$d\bar{p}_m(Q') = \bar{K}_s(Q')da \tag{2}$$

radiating in the presence of the perfectly-conducting surface, which covers the aperture as well, is the equivalent source of the electric field $d\bar{E}(P)$ at P in the region exterior to the surface; here da is an area element at Q'. It will be shown how the geometrical theory of diffraction may be used to calculate the incremental field $d\bar{E}(P)$. The electric field $\bar{E}(P)$ is then found by integrating over the aperture A shown in Fig. 1.

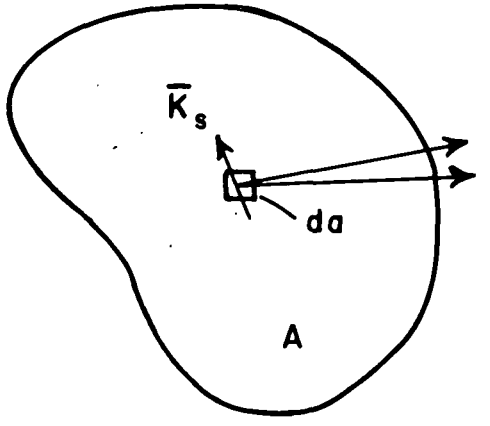

Fig. 1. The equivalent source in the aperture A.

According to geometrical optics the region exterior to a perfectly-conducting surface with a magnetic current moment at Q' is divided into an illuminated region and a shadow region by a plane tangent to the surface at Q'. This plane is referred to as the shadow boundary. A portion of these two regions adjacent to the shadow boundary is a transition region. The angular extent of the transition region is of the order $(k\rho_g)^{-1/3}$ in radians; ρ_g is the radius of curvature of the surface at Q' in the direction of the field point. The three regions are depicted in Fig. 2. We will describe how the high-frequency far-zone field may be calculated in the three regions. Let us begin with the field point P_3 in the shadow region (see Fig. 5).

A. Shadow Region

The equivalent magnetic current moment $\overline{K}_s da'$ at Q' excites waves which propagate along ray paths to the field point P; according to the generalized Fermat's principle proposed by Keller, the distance between Q' and P is an extremum (generally a minimum) on a ray path. With the field point at P_3 in the shadow region, see Fig. 2, it is evident that a part of the ray path which minimizes the distance between Q' and P_3 must lie on the perfectly-conducting surface, where it is a geodesic. In the case of simple surfaces such as the spherical surface, the cylindrical surface, the conical surface and the plane surface the geodesics are known and they are easy to describe; otherwise they can be found from the differential equations for the geodesic paths, which is a formidable but straightforward exercise; see Reference [25].

Now let us consider the behavior of the field associated with the surface ray (which we will henceforth refer to as the surface ray field):

$$a(t) = A(t)e^{j(\phi_0 - kt)} \tag{3}$$

in which A(t) is real, t is the distance along the surface ray, ϕ_0 is the phase at t=0, and a time dependence of $e^{j\omega t}$ is assumed and suppressed. As it propagates along a geodesic on the curved surface, the energy flux associated with this field is proportional to $A^2 d\eta$, where $d\eta$ is the infinitesimal distance between adjacent surface rays. It is assumed that the energy flux between adjacent surface rays is conserved. It follows from the generalized Fermat's principle that the surface ray sheds rays tangentially as it propagates; thus energy is continuously lost from the surface ray field, and it is attenuated. This may be expressed as

$$\frac{d}{dt}(A^2 d\eta) = -2\alpha(A^2 d\eta), \tag{4}$$

where α is the attenuation constant. The above equation is readily integrated between t_0 and t to give the surface ray field

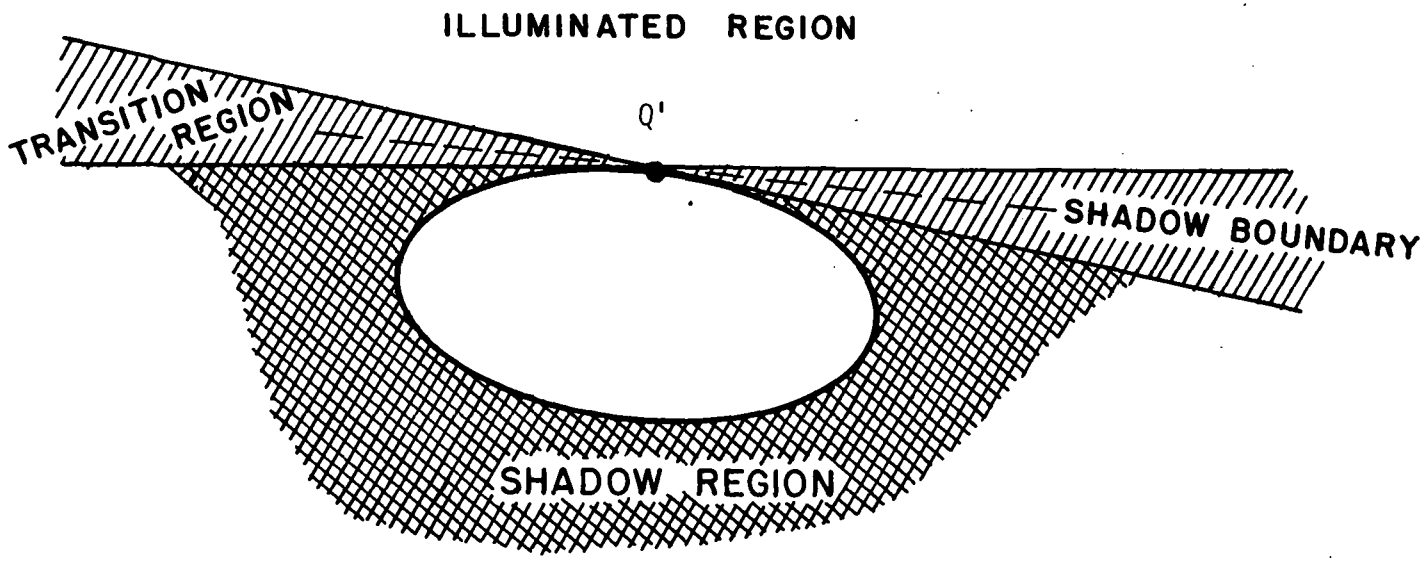

Fig. 2. Magnetic current moment on a curved surface showing the different regions of radiation.

$$a(t) = a(t_o)\sqrt{\frac{d\eta(t_o)}{d\eta(t)}}\, e^{-[jk(t-t_o)+\int_{t_o}^{t}\alpha(t')dt']} \qquad (5)$$

This expression must be modified when there is a caustic due to a point source on the surface at Q', where t=0. For t_o small $d\eta(t_o) = t_o d\psi_o$, where $d\psi_o$ is the angle between adjacent surface rays, see Fig. 3.

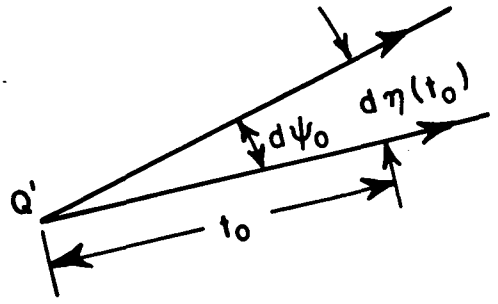

Fig. 3. The surface ray configuration close to a point source.

Moreover, a(t) must be independent of t_o; hence $\lim a(t_o)\sqrt{t_o}$ exists as $t_o \to 0$ and we define it to be C'. It follows then that

$$a(t) = C'\sqrt{\frac{d\psi_o}{d\eta}}\, e^{-[jkt + \int_{o}^{t}\alpha(t')dt']} \qquad (6)$$

The constant C' is proportional to the strength of the source at Q'. To facilitate the discussion of the vector source $d\bar{p}_m$ it is desirable to introduce the unit vector $\hat{n}$ which is normal to the convex surface at Q and the unit vector $\hat{t}$ which is tangent to the surface ray at Q, see Fig. 4. A similar pair of unit vectors $\hat{n}'$, $\hat{t}'$ may be defined at Q'. In addition, the unit vectors $\hat{b}=-\hat{n}x\hat{t}$ and $\hat{b}'=-\hat{n}'x\hat{t}'$ are defined at Q and Q', respectively. For the sake of simplicity, the following development is restricted to surface rays with zero torsion.

The source $d\bar{p}_m$ may be resolved into components parallel and perpendicular to the surface ray of interest at Q'. For surface rays with zero torsion, it is assumed that these two components induce surface ray fields which propagate independently of each other along the geodesic arc between Q' and Q. First let us consider the surface ray field excited by the component of the source $\hat{b} \cdot d\bar{p}_m$, which is perpendicular to the surface ray ($\hat{b}' = \hat{b}$ when the torsion vanishes). From canonical problems, it is found that $\hat{b} \cdot d\bar{p}_m$ excites an infinity

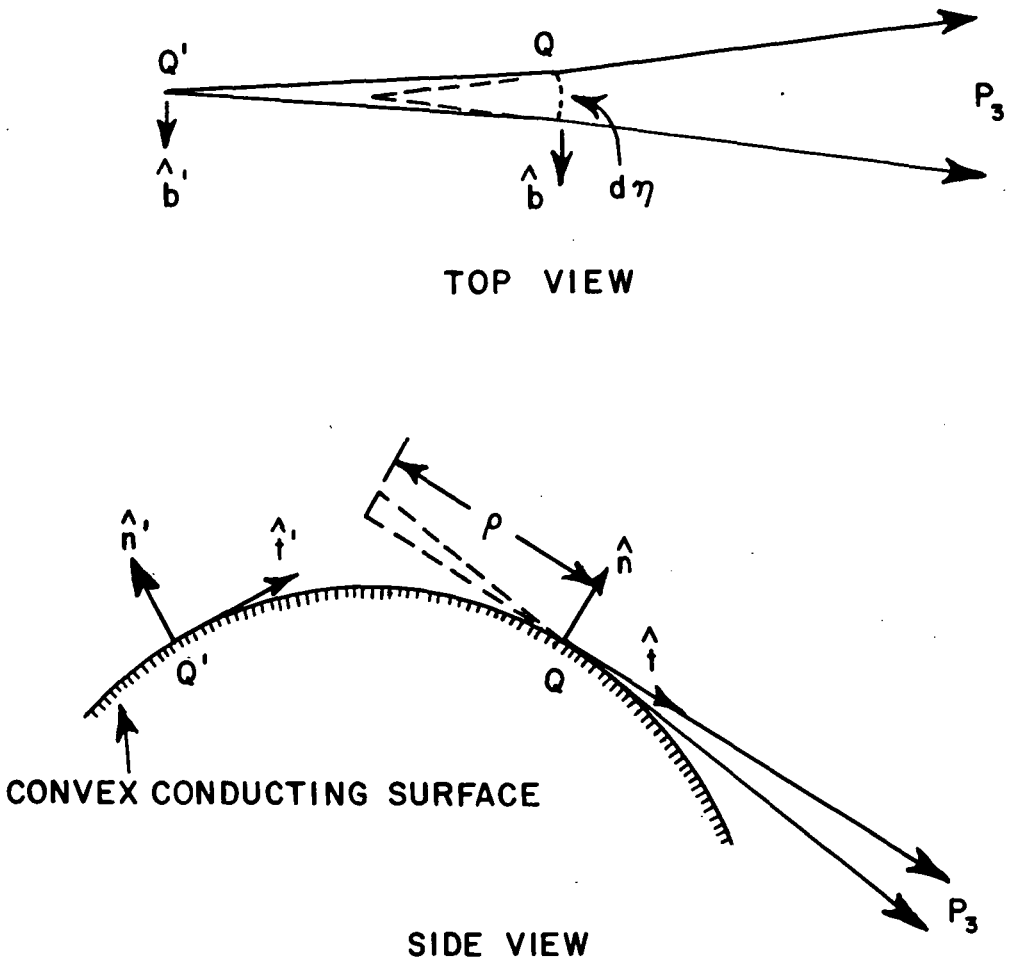

Fig. 4. Diffraction from a source Q' on a convex surface.

of surface ray modes, and that the electric field of each of these modes is perpendicular to the surface. It follows from Eq. (6) that this electric field

$$\hat{n} \cdot d\bar{E}_p(Q) = C'_p \sqrt{\frac{d\psi_o}{d\eta}}\, e^{-[jkt + \int_o^t \alpha_p^h(t')dt']}, \tag{7}$$

where α_p^h is the attenuation constant of the p^{th} mode for the hard boundary condition, where the normal derivative of the field vanishes

at the surface.* The superscript h on a quantity denotes that it is associated with the hard boundary condition. The point Q is at a distance t from Q' measured along the surface ray. The constant C'_p is proportional to $\hat{b} \cdot d\bar{p}_m$. The constant of proportionality is $C\, L_p^h$, where L_p^h is referred to as a launching coefficient and C is a conveniently chosen constant which is independent of p, so

$$C'_p = C\, L_p^h(Q')\, \hat{b} \cdot d\bar{p}_m(Q'). \tag{8}$$

We can now find the electric field of the p^{th} mode diffracted from Q toward P_3; this field is $\hat{n}$ directed. From Fig. 4 it is apparent that the convex surface is the locus of one of the caustics of the diffracted rays. The other caustic is at a distance of ρ from the surface, as shown in the figure. From the geometrical theory of diffraction

$$\hat{n} \cdot d\bar{E}_p(P_3) = \kappa_p \sqrt{\frac{\rho}{s(\rho+s)}}\; e^{-jks}, \tag{9}$$

where s is the distance between Q and P_3 and κ_p is a constant proportional to $\hat{n} \cdot d\bar{E}_p(Q)$. In this case the constant of proportionality is Keller's diffraction coefficient for the high-frequency diffraction by a curved surface; hence

$$\kappa_p = D_p^h(Q)\, \hat{n} \cdot d\bar{E}p(Q). \tag{10}$$

In the present development we are interested in the far-zone field where $s >> \rho$. Combining the results of Eqs. (7), (8), (9), and (10) and summing over the modes of the surface ray field, the electric field at P_3 due to the component of $d\bar{p}_m$ perpendicular to the surface ray is

$$\hat{n} \cdot d\bar{E}(P_3) = C\, \hat{b} \cdot d\bar{p}_m(Q')\, F(Q',Q)\, \frac{e^{-jks}}{s} \tag{11}$$

in which

$$F(Q',Q) = \sqrt{\frac{d\psi_o}{d\psi}} \sum_{p=0}^{\infty} L_p^h(Q') D_p^h(Q) e^{-\left[jkt + \int_0^t \alpha_p^h(t')dt'\right]}, \tag{12}$$

where $d\psi = d\eta/\rho$ is the angle between adjacent rays at Q.

---

*This approximation of the hard boundary condition for electromagnetic waves is adequate for the present discussion. A more complete treatment is given in Section IIIA.

Next let us consider the surface ray field excited by the component of the source $\hat{t}' \cdot d\bar{p}_m$ parallel to the surface ray of interest. This electric field is again perpendicular to the surface ray, but also tangent to the surface. In this case it is clear that the surface ray field does not represent the actual field at the boundary, since it must vanish there. The precise nature of this field in the boundary layer is unimportant, because the field is merely a convenient artifice to relate the field at Q to the source. The surface ray field does not appear in the final expression for the field at P_3.

Following the development used to treat the $\hat{b}'$-component of the source, one obtains

$$(13) \qquad \hat{b} \cdot d\bar{E}(P_3) = C\, \hat{t}' \cdot d\bar{p}_m(Q')\, G(Q',Q)\, \frac{e^{-jks}}{s}$$

as the $\hat{b}$ component of the electric field at P_3, where

$$(14) \qquad G(Q',Q) = \sqrt{\frac{d\psi_o}{d\psi}} \sum_{p=0}^{\infty} L_p^s(Q') D_p^s(Q)\, e^{-\left[jkt + \int_0^t \alpha_p^s(t')dt'\right]}$$

in which α_p^s, L_p^s, and D_p^s are the attenuation constant, launching coefficient and diffraction coefficient of the p^{th} mode for the soft boundary condition, where the field vanishes at the surface.

One may combine Eqs. (11) and (13) to obtain the far-zone field at P_3 due to the magnetic current moment $d\bar{p}_m$ at Q'

$$(15) \qquad d\bar{E}(P_3) = C\, d\bar{p}_m(Q') \cdot [\hat{b}\, \hat{n}\, F(Q',Q) + \hat{t}'\, \hat{b}\, G(Q',Q)]\, \frac{e^{-jks}}{s} .$$

The attenuation constants, launching coefficients and diffraction coefficients which appear in the expressions for F and G are found from the asymptotic solution of canonical problems. The constant C also may be found from these solutions. The preceding discussion does not take into account the effect of surface ray fields which have encircled a closed surface ℓ times. The inclusion of these fields is straightforward; one only needs to sum a power series in ℓ, where the phase jumps at any caustics which have been crossed in an encirclement are taken into account. Since this phase jump equals $\pi/2$ each time the caustic is crossed, it is easily taken into account by introducing a factor of j. Usually the contribution from the multiply-encircling waves is insignificant, unless the closed ray path is a few wavelengths or less. Also, in the case of a closed smooth surface there is generally diffraction from two points toward the field point; these are shown as points Q_1 and Q_2 in Fig. 5.

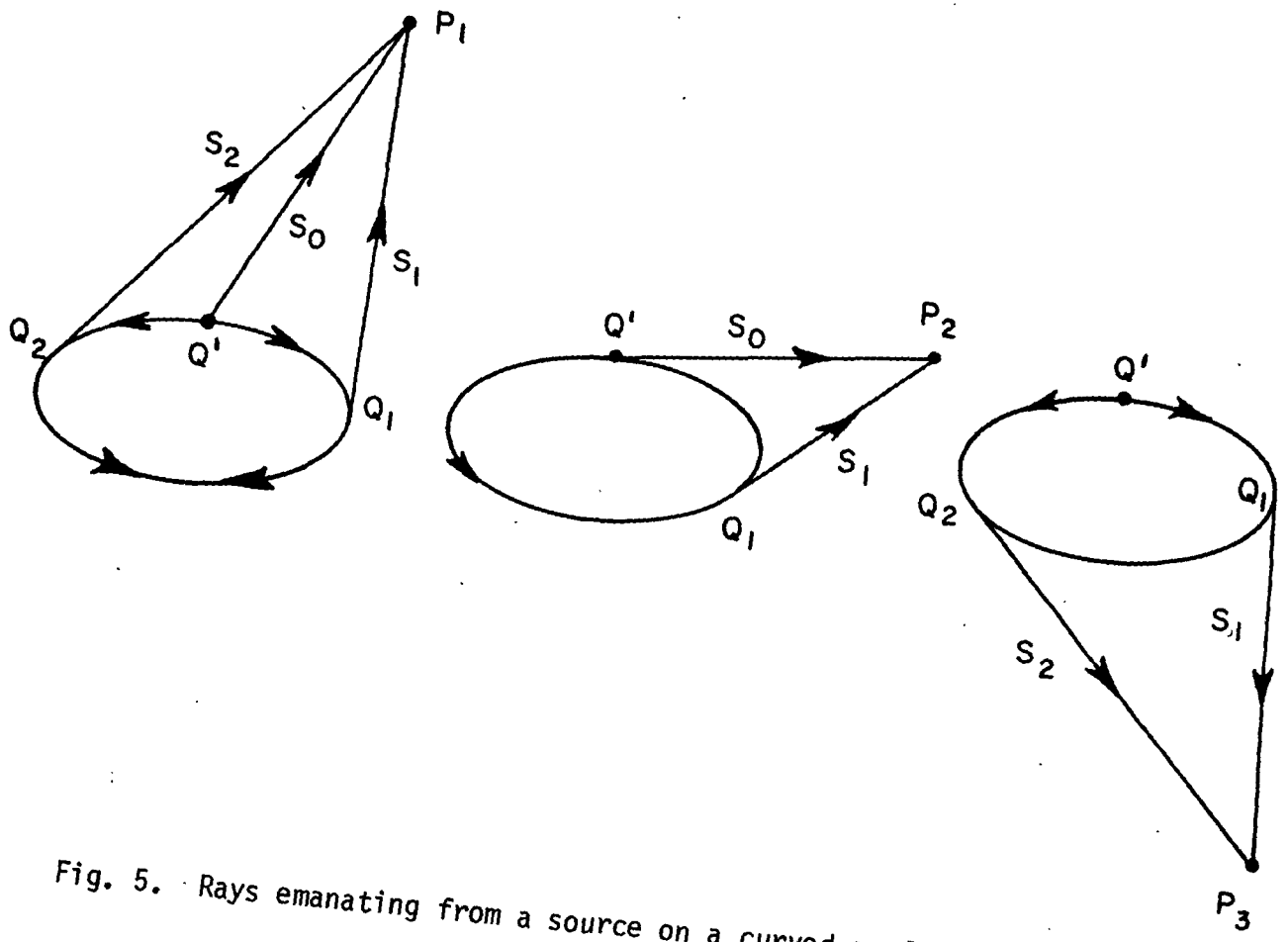

Fig. 5. Rays emanating from a source on a curved surface.

If the field point occurs at a caustic of the diffracted rays, so that infinitely many diffracted rays pass through P_3, the geometrical theory of diffraction solution fails. However, it may be supplemented by an appropriate integral representation of the field, where the geometrical theory of diffraction is used to determine the equivalent sources of the integral representation. This is described in Appendix III.

B. Transition Region

The series representations for F and G in Eqs. (12) and (14) are rapidly convergent when the field point is deep in the shadow region. Usually only the first few terms are required to achieve reasonable accuracy, when the radii of curvature of the surface are larger than a wavelength or so. However as P_3 moves toward the transition region more terms must be added to maintain accuracy. As the field point moves into the transition region, the point Q approaches close to Q' and it is no longer desirable to treat the excitation, propagation and diffraction of the different surface ray modes separately. As a result, the series representations for the functions F and G are replaced by integral representations, and these functions are found to be proportional to the Fock functions used to describe "creeping waves" in the asymptotic theory of plane wave diffraction by curved surfaces. From the viewpoint of reciprocity this result is to be expected; more will be said about this later.

Also as Q approaches Q', one notes that

$$\frac{d\psi_o}{d\psi} \to 1 \ .$$

The ray configuration for a closed surface is shown in Fig. 5. The field of the ray $Q'P_2$ is calculated from the integral representations of F and G; on the other hand, ray $Q'Q_1P_2$ is seen to have a considerable excursion on the surface and so the field of this ray is better calculated using Eqs. (12) and (14).

C. Illuminated Region

If the field point is at P_1 in the illuminated region, the radiation from the source at Q' propagates along a straight line to P_1. According to geometrical optics, the electric field at P_1 due to the magnetic current moment $d\bar{p}_m$ at Q' is

$$\bar{E}(P_1) = \frac{jk}{2\pi} \hat{s} \times d\bar{p}_m(Q') \frac{e^{-jks}}{s} \ , \qquad (16)$$

where $\hat{s}$ is a unit vector directed from Q' to P_1, as shown in Fig. 6. This equation may be written in a form similar to that employed when

the field point is in the shadow and transition regions, see Eq. (15); we proceed as follows.

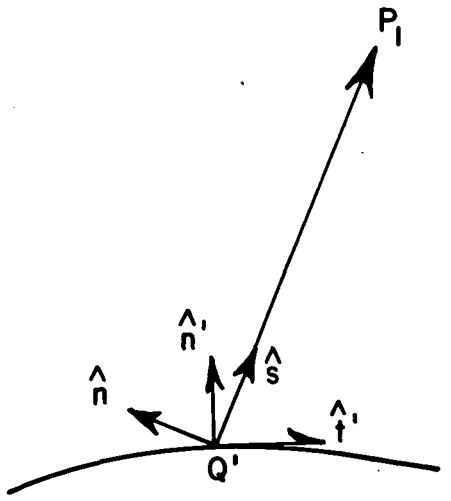

Fig. 6. An incident ray in the illuminated region.

First let us define a plane of incidence which contains $\hat{s}$ and $\hat{n}'$, the unit vector normal to the surface at Q'. The unit vectors associated with the field, which are normal to the ray $Q'P_1$ and parallel and perpendicular to the plane of incidence are $\hat{n}$ and $\hat{b}$, respectively. The unit vectors associated with the source, which are tangent to the surface at Q' and parallel and perpendicular to the plane of incidence are t' and $\hat{b}$, respectively.

It follows from Eq. (16) that

$$(17) \qquad d\bar{E}(P_1) = C\, d\bar{p}_m(Q') \cdot [\hat{b}\,\hat{n}\,2 + \hat{t}'\,\hat{b}\,2\cos\theta]\,\frac{e^{-jks}}{s}$$

in which $\cos\theta = \hat{n}'\cdot\hat{s}$. From the equation above we see that

$$(18a,b) \qquad F = 2 \quad \text{and} \quad G = 2\cos\theta$$

according to geometrical optics. This approximation is found to be reasonably accurate deep in the illuminated region where

$$\theta < \frac{\pi}{2} - [k\rho_g(Q')]^{-1/3}.$$

It joins smoothly with representations for the transition region, which are described in the next chapter.

In the case of the closed surface shown in Fig. 5, the fields of the rays emanating from Q' and subsequently diffracted from the points Q_1 and Q_2 are also included in the calculation of the field at P_1. These fields would be calculated from Eqs. (12), (14) and (15).

It was noted earlier that ray optical approximations satisfy the reciprocity principle. This can be confirmed for the solution just described. Let $\overline{H}(Q',P)$ be the magnetic field at Q' on the surface due to a unit magnetic current moment $\hat{u}$ at the exterior point P. This field can be found from an asymptotic solution of the diffraction problem posed by the perfectly-conducting curved surface. Let $\overline{H}(P,Q')$ be the magnetic field at P due to the differential magnetic current moment $d\overline{p}_m$ at Q'. According to the reciprocity principle,

$$\hat{u} \cdot \overline{H}(P,Q') = \overline{H}(Q',P) \cdot d\overline{p}_m \quad . \tag{19}$$

It is found that expressions for the $\hat{u}$-component of the magnetic field determined from the above equation are the same as those found from our application of the geometrical theory of diffraction. This checks the present development and shows that it is consistent with the reciprocity principle.

D. Two-Dimensional Geometries

The preceding development is easily modified so that it can be applied to 2-dimensional geometries involving infinitely long axial slots in the surfaces of perfectly-conducting cylinders. The tangential electric field in these slots may be axial E_z or transverse E_t, or a linear combination of the two. Thus two types of infinitesimal elementary sources at Q' are of interest: a line of axial magnetic current

$$dM_z(Q') = \pm \hat{t}' \cdot d\overline{E}(Q')dt' \tag{20}$$

which is an ordinary magnetic line current flowing parallel to the z axis, or a linear distribution in the z-direction of magnetic current elements which are transversely directed,

$$dM_t(Q') = \hat{b} \cdot d\overline{E}(Q')dt' \tag{21}$$

Note that $\hat{b} = \pm \hat{z}$ here and dt' is an infinitesimal circumferential distance at Q'. In each case the upper sign is used if $\hat{t}$ is directed in the clockwise sense, the lower sign is used, if in the counterclockwise sense.

Many 2-dimensional problems of this type have been treated rigorously, so they may be used to check the accuracy of our GTD solution. Moreover, where asymptotic solutions exist, they may be used as canonical problems from which the parameters of the GTD solution can be found. Also such geometries are of interest, because their patterns are the same as those of finite axial and circumferential slots in cylinders, when the patterns are calculated in the symmetry plane perpendicular to the axis of the cylinder.

The surface rays emanating from the line source excitation are parallel so

$$\frac{d\psi_o}{d\psi} = 1 \tag{22}$$

in Eqs. (12) and (14), and the amplitude variation along the ray shed tangentially from the surface ray to the field point is $s^{-1/2}$. In general

$$d\bar{M} = \hat{z}dM_z + \hat{t}'dM_{t'} \tag{23}$$

consequently, the two-dimensional form of Eq. (15) is

$$d\bar{E}(P_3) = C\, d\bar{M}\cdot[\hat{b}\hat{n}F(Q',Q) + \hat{t}'\hat{b}\, G(Q',Q)]\, \frac{e^{-jks}}{\sqrt{s}}\,, \tag{24}$$

in which the normalizing constant C may be expected to have a value different from that in Eq. (15). Both values of C are found from the solutions of canonical problems, and $\hat{b} = \pm \hat{z}$ as noted earlier.

III. THE PARAMETERS AND TRANSITION FUNCTIONS

Expressions for the diffraction coefficients, attenuation constants and launching coefficients used in Eqs. (12) and (14) are given in this section along with the integral representations for the functions F and G employed in the transition region. The manner in which these integral representations transform to the geometrical optics field and the residue series used in the illuminated and shadowed regions is discussed.

A. Diffraction Coefficients and Attenuation Constants

The diffraction coefficients and attenuation constants depend on the local geometry of the surface, the wave number k, and the nature of the surface as described by the boundary conditions. Keller and Levy[7] have given the first order terms in the expressions for the diffraction coefficients and attenuation constants. However, before we present their results, it is desirable to examine the terms "soft" and "hard" boundary conditions mentioned in the preceding chapter.

This terminology is borrowed from acoustics. A soft boundary is one where the pressure field vanishes at the surface; it is also referred to as a Dirichlet boundary. On the other hand, a hard boundary is one where the normal derivative of the pressure field vanishes at the surface; this is also referred to as a Neumann boundary. Two types of surface ray modes have been assumed. For one type the electric field is in the binormal direction so that $\bar{E}_p = b\, E_p$, and for the other, the magnetic field is in the binormal direction so that $\bar{H}_p = \hat{b}\, H_p$, and there is a normally-directed electric field $\hat{n} \cdot \bar{E}_p$. The binormally directed electric field clearly satisfies a soft or Dirichlet boundary condition at the surface, whereas the binormally-directed magnetic field satisfies the boundary condition

$$\frac{\partial H}{\partial n} + \left(\frac{1}{h_b}\frac{\partial h_b}{\partial n}\right) H = 0. \tag{25}$$

in which h_b is the metrical coefficient associated with the unit vector b. The above boundary condition describes what we will refer to as a hard EM boundary. At high frequencies the second term is relatively small, so that the surface ray magnetic field satisfies a hard or Neumann boundary condition to a first approximation. Also Eq. (25) reduces to the hard boundary condition in the case of cylindrical surfaces where $h_b = 1$. These observations concerning the boundary conditions are of importance in the paragraphs to follow.

Let ρ_g be the radius of curvature of the surface along which the surface ray is propagating in the plane containing the normal to the surface and the tangent to the surface ray. As mentioned earlier, Keller and Levy[7] have used first order asymptotic solutions for the diffraction of acoustic (scalar) and electromagnetic waves to deduce the attenuation constants and diffraction coefficients. For these canonical problems $\rho_g = a$, a constant. According to Keller and Levy

$$\alpha_{op}^{s} = \frac{1}{a}\left(\frac{ka}{2}\right)^{1/3} q_p\, e^{j\frac{\pi}{6}} \tag{26}$$

$$[D_{op}^{s}]^2 = \frac{e^{-j\frac{\pi}{12}}}{2^{5/6}\pi^{1/2}(ka)^{1/6}} \frac{a^{1/2}}{[Ai'(-q_p)]^2} \tag{27}$$

for the soft surface, and

$$\alpha_{op}^{h} = \frac{1}{a}\left(\frac{ka}{2}\right)^{1/3} \bar{q}_p\, e^{j\frac{\pi}{6}} \tag{28}$$

$$(29) \qquad [D_{op}^{h}]^2 = \frac{e^{-j\frac{\pi}{12}}}{2^{5/6}\pi^{1/2}(ka)^{1/6}} \frac{a^{1/2}}{\bar{q}_p} \frac{}{[Ai(-\bar{q}_p)]^2}$$

for the hard surface, where the Miller-type Airy function[11] is given by

$$(30) \qquad Ai(-x) = \frac{1}{\pi}\int_0^{\infty} \cos(\tfrac{1}{3}t^3 - xt)\, dt,$$

$$(31) \qquad Ai(-q_p) = 0,$$

$$(32) \qquad Ai'(-\bar{q}_p) = 0,$$

and the prime denotes differentiation with respect to the argument of the function.

Voltmer[9] employing the same canonical problems as Keller and Levy, obtained attenuation constants and diffraction coefficients of improved accuracy by retaining higher order terms in the asymptotic solutions. Voltmer's results are presented in Table I, where it is seen that the corrections to the attenuation constants and diffraction coefficients are of order $(2/ka)^{2/3}$.

The first order approximations given by Eqs. (26) to (29) do not depend on whether the surface is cylindrical or spherical or on whether the wave is acoustic or electromagnetic. From Table I it is evident that this is no longer the case with the more accurate formulas. However an explanation of these second order differences is best accomplished after examining the high frequency diffraction by a more general surface, i.e., a surface of variable curvature along the ray path or of arbitrary curvature transverse to the ray path.

Keller and Levy[15], Franz and Klante[21], Hong[10] and Voltmer[9] have considered the high frequency diffraction by general convex surfaces. Hong has obtained asymptotic solutions to the integral equations for the plane wave diffraction by a hard acoustic surface and the plane wave diffraction by a hard EM boundary. Voltmer has extended this work to soft boundaries, which are the same for acoustic and EM waves as we have noted. The solutions were carried out to second order, and they are functions not only of ρ_g, the radius of curvature of the surface with respect to arc length along the ray trajectory, but also $\dot{\rho}_g$, $\ddot{\rho}_g$ and ρ_{tn}, where the dot denotes a derivative with respect to arc length along the ray trajectory and ρ_{tn} is the radius of curvature of the surface in the direction of the binormal to the ray. Expressions for the attenuation constants are evident from the solutions; these are tabulated in columns C and D of Table II. On the

TABLE I

DIFFRACTION COEFFICIENTS AND ATTENUATION CONSTANTS FOR CIRCULAR CYLINDERS AND SPHERES

Surface	SQUARE OF DIFFRACTION COEFFICIENT D_p^2 = (Column A) · (Column B)		ATTENUATION CONSTANT α_p = (Column C) · (Column D)		ZEROES OF THE AIRY FUNCTION
	A. Keller's Result	B. Correction Terms	C. Keller's Result	D. Correction Terms	
Soft Cylinder	$\dfrac{\pi^{-1/2}2^{-5/6}a^{1/3}e^{-j\pi/12}}{k^{1/6}(Ai'(-q_p))^2}$	$1 + \left(\dfrac{2}{ka}\right)^{2/3} q_p \dfrac{1}{30} e^{-j\pi/3}$	$\dfrac{q_p}{a} e^{j\pi/6} \left(\dfrac{ka}{2}\right)^{1/3}$	$1 + \left(\dfrac{2}{ka}\right)^{2/3} \dfrac{q_p}{60} e^{-j\pi/3}$	$Ai(-q_p) = 0$ $q_1 = 2.33811$ $q_2 = 4.08795$ $Ai'(-q_1) = .70121$ $Ai'(-q_2) = -.80311$
Soft Acoustic and Soft EM Sphere		$1 + \left(\dfrac{2}{ka}\right)^{2/3} q_p \left(\dfrac{1}{30} + \dfrac{1}{4}\right) e^{-j\pi/3}$			
Hard Cylinder	$\dfrac{\pi^{-1/2}2^{-5/6}a^{1/3}e^{-j\pi/12}}{k^{1/6}\bar{q}_p(Ai(-\bar{q}_p))^2}$	$1 + \left(\dfrac{2}{ka}\right)^{2/3} \left(\dfrac{\bar{q}_p}{30} - \dfrac{1}{\bar{q}_p^2} \dfrac{1}{10}\right) e^{-j\pi/3}$	$\dfrac{\bar{q}_p}{a} e^{j\pi/6} \left(\dfrac{ka}{2}\right)^{1/3}$	$1 + \left(\dfrac{2}{ka}\right)^{2/3} \left(\dfrac{\bar{q}_p}{60} + \dfrac{1}{\bar{q}_p^2} \dfrac{1}{10}\right) e^{-j\pi/3}$	$Ai'(-\bar{q}_p) = 0$ $\bar{q}_1 = 1.01879$ $\bar{q}_2 = 3.24820$ $Ai(-\bar{q}_1) = .53566$ $Ai(-\bar{q}_2) = -.41902$
Hard Acoustic Sphere		$1 + \left(\dfrac{2}{ka}\right)^{2/3} \left(\bar{q}_p\left(\dfrac{1}{30} + \dfrac{1}{4}\right) - \dfrac{1}{\bar{q}_p^2}\left(\dfrac{1}{10} + \dfrac{1}{4}\right)\right) e^{-j\pi/3}$		$1 + \left(\dfrac{2}{ka}\right)^{2/3} \left(\dfrac{\bar{q}_p}{60} + \dfrac{1}{\bar{q}_p^2}\left(\dfrac{1}{10} + \dfrac{1}{4}\right)\right) e^{-j\pi/3}$	
Hard Em Sphere		$1 + \left(\dfrac{2}{ka}\right)^{2/3} \bar{q}_p \left(\dfrac{1}{30} + \dfrac{1}{4}\right) - \dfrac{1}{\bar{q}_p^2}\left(\dfrac{1}{10} - \dfrac{1}{4}\right)\right) e^{-j\pi/3}$		$1 + \left(\dfrac{2}{ka}\right)^{2/3} \left(\dfrac{\bar{q}_p}{60} + \dfrac{1}{\bar{q}_p^2}\left(\dfrac{1}{10} - \dfrac{1}{4}\right)\right) e^{-j\pi/3}$	

TABLE II

GENERALIZED DIFFRACTION COEFFICIENTS AND ATTENUATION CONSTANTS

Surface	SQUARE OF DIFFRACTION COEFFICIENT D_p^2 = (Column A) · (Column B)		ATTENUATION CONSTANT α_p = (Column C) · (Column D)	
	A. Keller's Result	B. Correction Terms	C. Keller's Result	D. Correction Terms
Soft Acoustic and Soft EM	$\frac{\pi^{-1/2}2^{-5/6}\rho_g^{1/3}e^{-j\pi/12}}{k^{1/6}(Ai'(-q_p))^2}$	$1+\left(\frac{2}{k\rho_g}\right)^{2/3} q_p\left(\frac{1}{30}+\frac{\rho_g}{4\rho_{tn}}+\cdots\right)e^{-j\pi/3}$	$\frac{q_p}{\rho_g}e^{j\pi/6}\left(\frac{k\rho_g}{2}\right)^{1/3}$	$1+\left(\frac{2}{k\rho_g}\right)^{2/3} q_p\left(\frac{1}{60}-\frac{2}{45}\rho_g\dot{\rho}_g+\frac{4}{135}\dot{\rho}_g^2\right)e^{-j\pi/3}$
Hard Acoustic	$\frac{\pi^{-1/2}2^{-5/6}\rho_g^{1/3}e^{-j\pi/12}}{k^{1/6}\bar{q}_p(Ai(-\bar{q}_p))^2}$	$1+\left(\frac{2}{k\rho_g}\right)^{2/3}\left(\bar{q}_p\left(\frac{1}{30}+\frac{\rho_g}{4\rho_{tn}}+\cdots\right)-\frac{1}{\bar{q}_p^2}\left(\frac{1}{10}+\frac{\rho_g}{4\rho_{tn}}+\cdots\right)\right)e^{-j\pi/3}$	$\frac{\bar{q}_p}{\rho_g}e^{j\pi/6}\left(\frac{k\rho_g}{2}\right)^{1/3}$	$1+\left(\frac{2}{k\rho_g}\right)^{2/3}\left(\bar{q}_p\left(\frac{1}{60}-\frac{2}{45}\rho_g\dot{\rho}_g+\frac{4}{135}\dot{\rho}_g^2\right)+\frac{1}{\bar{q}_p^2}\left(\frac{1}{10}+\frac{\rho_g}{4\rho_{tn}}-\frac{\rho_g\dot{\rho}_g}{60}+\frac{\dot{\rho}_g^2}{90}\right)\right)e^{-j\pi/3}$
Hard EM		$1+\left(\frac{2}{k\rho_g}\right)^{2/3}\left(\bar{q}_p\left(\frac{1}{30}+\frac{\rho_g}{4\rho_{tn}}+\cdots\right)-\frac{1}{\bar{q}_p^2}\left(\frac{1}{10}-\frac{\rho_g}{4\rho_{tn}}+\cdots\right)\right)e^{-j\pi/3}$		$1+\left(\frac{2}{k\rho_g}\right)^{2/3}\left(\bar{q}_p\left(\frac{1}{60}-\frac{2}{45}\rho_g\dot{\rho}_g+\frac{4}{135}\dot{\rho}_g^2\right)+\frac{1}{\bar{q}_p^2}\left(\frac{1}{10}-\frac{\rho_g}{4\rho_{tn}}-\frac{\rho_g\dot{\rho}_g}{60}+\frac{\dot{\rho}_g^2}{90}\right)\right)e^{-j\pi/3}$

ρ_g = radius of curvature along the geodesic

ρ_{tn} = radius of curvature perpendicular to the geodesic (transverse curve)

Dots indicate differentiation with respect to arc length variable

other hand, complete expressions for the diffraction coefficients can not be obtained from these solutions, because $\dot{\rho}_g$ is assumed to be zero at the point of incidence on the surface, where the diffraction coefficient is evaluated. This condition was imposed to simplify the pertinent integral equations. The best available diffraction coefficients (more precisely, the diffraction coefficients squared) are given in Columns A and B of Table II. The incomplete portion of the second order term is indicated by (...); it is a function of $\dot{\rho}_g$ and $\ddot{\rho}_g$.* In deriving these results it is assumed that $\rho_g/\rho_{tn} > 1$; furthermore as in the last chapter, it is assumed that the surface rays have no torsion.

It is believed that the attenuation constants and diffraction coefficients listed in Table II are the best available at present and that they are adequate for most calculations, even though the expressions for the diffraction coefficient are not complete to second order. The improved attenuation constants are very important, because of the sensitivity of numerical calculations to errors in these parameters; corresponding errors in the diffraction coefficient are clearly less important to numerical accuracy.

It is interesting to examine the general behavior of the attenuation constants and diffraction coefficients listed in Tables I and II. It is noted that all the corrections to the first order expressions of Keller and Levy are of order $(2/k\rho_g)^{2/3}$, and so their importance increases with a decrease in the radius of curvature of the surface with respect to wavelength. All of the formulas in Table II reduce to those in Table I for the cylindrical and spherical surface, which is an important check on the asymptotic solution for the more general convex surface. The distinction between cylindrical and spherical surfaces in Table I is not required in Table II, because the term $\rho_g/4\rho_{tn}$ takes care of this difference; $\rho_g = \rho_{tn} = a$ for the sphere, whereas ρ_{tn} is infinite for circumferential rays on the cylinder. The formulas for the soft acoustic and soft EM surfaces are the same; this is expected because the boundary conditions are identical. On the other hand, the formulas for the attenuation constants and diffraction coefficients associated with the hard acoustic and hard EM surfaces are different, because the boundary conditions at the two surfaces are different.

B. Launching Coefficients and Constants

The launching coefficients have been defined in Eqs. (8) and (14). To determine the launching coefficients the radiation from a magnetic current moment on a perfectly-conducting sphere and the radiation from magnetic current line sources on cylindrical surfaces have been analyzed. The asymptotic solution of these canonical problems and

*The $\dot{\rho}_g$ and $\ddot{\rho}_g$ terms in the diffraction coefficient will be the subject of a future investigation.

their ray optical interpretation is described in Appendix I, where it is found that for both cylindrical and spherical surfaces

$$(33) \qquad L_p^s = - (jk\tfrac{\pi}{2})^{1/2} H_{\nu_p}^{(2)'}(ka)\, D_p^s,$$

$$(34) \qquad L_p^h = - j(jk\tfrac{\pi}{2})^{1/2} H_{\nu_p}^{(2)}(ka)\, D_p^h,$$

where ν_p are the zeroes of the Hankel function in the first equation and the zeroes of the derivative of the Hankel function in the second equation. It is apparent that the relationship of the launching coefficient to the diffraction coefficient does not depend on the surface curvature transverse to the ray direction. For this reason, one may assume that

$$(35) \qquad L_p^s = e^{-j\frac{\pi}{12}}(2\pi k)^{1/2}(\frac{2}{k\rho_g})^{2/3} Ai'(-q_p)\left[1 - (\frac{2}{k\rho_g})^{2/3} \frac{q_p}{15} e^{j\frac{2\pi}{3}}\right] D_p^s$$

$$(36) \qquad L_p^h = e^{j\frac{\pi}{12}}(2\pi k)^{1/2}(\frac{2}{k\rho_g})^{1/3} Ai(-\bar{q}_p)\left[1 + (\frac{2}{k\rho_g})^{2/3} \frac{\bar{q}_p}{15} e^{j\frac{2\pi}{3}}\right] D_p^h$$

These expressions for the launching coefficients, where D_p^s and D_p^h are obtained from Table II, are the best available at present. It would be desirable to solve a canonical problem where the magnetic current moment or line source is on a surface of variable curvature as a further check.

From Eqs. (A-26), (A-36) and (A-59) in Appendix I it is found that the constant

$$(37a,b) \qquad C = \begin{cases} \dfrac{-jk}{4\pi} & \text{for 3-dimensional problems, see Eq. (15)} \\ \dfrac{-ke^{j\frac{\pi}{4}}}{\sqrt{8\pi k}} & \text{for 2-dimensional problems, see Eq. (24)} \end{cases}$$

We note that C also could have been found from the geometrical optics expressions, i.e., from Eqs. (16), (17) and (18) for the 3-dimensional geometries, and from Eqs. (24) and (18) for the 2-dimensional geometries.

C. Integral Representations for the Transition Region

In the transition region which exists on either side of the shadow boundary, an integral representation for the field is necessary because the series representation for the F and G functions becomes poorly convergent; this integral representation yields a smooth transition for the radiation field from the shadow region, where the surface ray modes are employed, to the illuminated region, where the geometrical optics field is used. As mentioned earlier, the angular extent of the transition region on each side of the shadow boundary is of order $(k\rho_g)^{-1/3}$. The expressions for the fields in the transition region are also deduced from the asymptotic solutions to appropriate canonical problems as described in Appendix II, and it is pointed out there that a first order approximation is usually adequate in the transition region.

The integral representations for the field in the transition region can be expressed in terms of the well-tabulated Fock functions[22]:

1) hard Fock function

$$g(\xi) = \frac{1}{\sqrt{\pi}} \int_{\Gamma_1} \frac{e^{-j\tau\xi}}{w_2'(\tau)} \, d\tau, \tag{38}$$

2) soft Fock function

$$\tilde{g}(\xi) = \frac{1}{\sqrt{\pi}} \int_{\Gamma_1} \frac{e^{-j\tau\xi}}{w_2(\tau)} \, d\tau, \tag{39}$$

which are described in Appendix II.

Consider an infinitesimal portion of a surface ray on a perfectly-conducting surface of variable curvature. It follows from the work of Fock[23], Wetzel[24] and Goodrich[5] that the variation of the field over this ray increment dt, and hence the variation of $g(\xi)$ or $\tilde{g}(\xi)$, behaves as though the surface were locally that of a cylinder or sphere, with a radius equal to that of the local radius of curvature in the direction of the ray ρ_g. Hence

$$\frac{dg}{dt} = g'(\xi) \frac{d\xi}{dt} \quad \text{or} \quad \frac{d\tilde{g}}{dt} = \tilde{g}'(\xi) \frac{d\xi}{dt}, \tag{40a,b}$$

where

$$(41) \qquad \frac{d\xi}{dt} = \frac{1}{\rho_g}\left(\frac{k\rho_g}{2}\right)^{1/3},$$

which is deduced from Eq. (A-71) after noting that $ad\psi = dt$.

Generalizing F and G as given by Eqs. (A-79) and (A-92) in this manner for the 2-dimensional case

$$(42) \qquad F = g(\xi)\, e^{-jkt}$$

$$(43) \qquad G = -j\left(\frac{2}{k\rho_g(t)}\right)^{1/3} \tilde{g}(\xi) f(t) e^{-jkt}$$

in which

$$(44) \qquad \xi = \int_0^t \frac{1}{\rho_g}\left(\frac{k\rho_g}{2}\right)^{1/3} dt'$$

follows from Eq. (41) and t is the distance between Q and Q', see Fig. 4.

ξ, $t > 0$ when the field point is below the shadow boundary in the shadow region, and ξ, $t < 0$ when the field point is above the shadow boundary in the illuminated region, as shown in Fig. 7. When the field point is in the illuminated portion of the transition region, one visualizes the surface ray as traveling from its source at Q' to Q_1, where it sheds tangentially back toward P. The Q' Q_1 P ray path does not obey the generalized Fermat's principle and therefore it is a pseudo ray system, but it does serve as a useful coordinate system to calculate the field at P in the illuminated part of the transition region.

The function f(t) appearing in Eq. (43), is given by

$$(45) \qquad f(t) = \begin{cases} 1 & , \quad -1 < \hat{n}' \cdot \hat{s} \leq 0 \\ \dfrac{\hat{n}' \cdot \hat{s}}{\left(\frac{2}{k\rho_g(t)}\right)^{1/3} \int_0^t \frac{1}{\rho_g}\left(\frac{k\rho_g}{2}\right)^{1/3} dt'} & , \quad 0 \leq \hat{n}' \cdot s < 1 \end{cases} .$$

The introduction of f(t) into Eq. (43) gives us an algorithm for calculating the field in the transition region; furthermore this field

joins smoothly with the geometrical optics field deep in the illuminated region. The accuracy of the algorithm has been confirmed by applying it to a number of examples. f(t) reduces to Eq. (A-93) for surfaces of constant curvature, i.e., the cylinder and sphere.

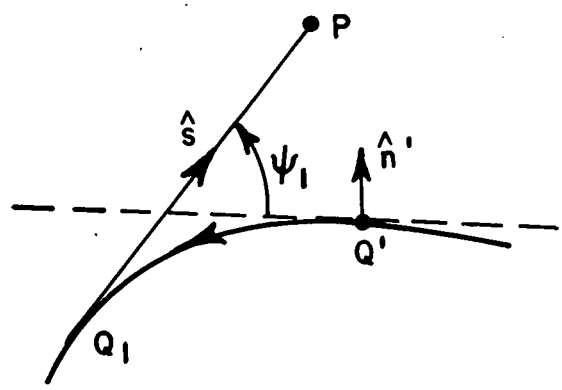

Fig. 7. An equivalent ray system for the field calculation in the illuminated part of the transition region.

In the case of 3-dimensional geometries

$$F = \begin{cases} \sqrt{\frac{d\psi_o}{d\psi}}\, g(\xi)e^{-jkt}, & t \geq 0, \quad \text{shadow region} \\ g(\xi)e^{-jkt}, & t \leq 0, \quad \text{illuminated region} \end{cases} \tag{46}$$

$$G = \begin{cases} -j\sqrt{\frac{d\psi_o}{d\psi}}\left(\frac{2}{k\rho_g(t)}\right)^{1/3} \tilde{g}(\xi)e^{-jkt}, & t \geq 0, \quad \text{shadow region} \\ -j\left(\frac{2}{k\rho_g(t)}\right)^{1/3} \tilde{g}(\xi)f(t)e^{-jkt}, & t \leq 0, \quad \text{illuminated region} \end{cases} \tag{47}$$

where ξ is given by Eq. (44), and the factor $d\psi_o/d\psi$ is defined in Section I, see Figs. 3 and 4. In Fig. 4 recall that $\rho d\psi = d\eta$. This factor measures the change in angle between adjacent surface rays as they propagate from their source point to the point of diffraction $Q_{1,2}$. If $d\psi_o/d\psi > 1$ the surface rays converge and if $d\psi_o/d\psi < 1$, they diverge. $d\psi_o/d\psi$ is a function of both the ray and surface geometries; it may be found by using differential geometry.

At first glance it may seem strange that $\sqrt{d\psi_0/d\psi}$ is not included in the expressions for the illuminated region. This may be explained with the aid of Fig. 7, where it is seen that the surface divergence of the rays emanating from the source to the point Q_1 is compensated by the subsequent convergence of the rays shed from Q_1 to the field point P in the far-zone.

Equations. (42), (43), (46) and (47) also may be joined in the transition region with the corresponding surface ray mode expressions for F and G, see Eqs. (12) and (14). Noting that the former equations are a first order asymptotic approximation, whereas the surface ray mode expressions are approximated roughly to second order here, one would expect small differences in the values calculated from the two representations in their common domain of validity; however these differences should not exceed a few tenths of a dB in most cases. Deep in the shadow region the surface ray mode expressions are definitely to be preferred.

The following summary of formulas is presented for the convenience of the reader. It also facilitates the discussion in the next section.

$$\Delta = [k\rho_g(Q')]^{-1/3}$$

in which $\rho_g(Q')$ is the curvature of the surface at the source Q' in the direction of the surface ray.

(a) Three-dimensional problems:

(2) $$d\bar{p}_m(Q') = [\bar{E}(Q') \times \hat{n}']da',$$

(15) $$d\bar{E}(P) = \frac{-jk}{4\pi} dp_m(Q') \cdot [\hat{b}\,\hat{n}\,F + \hat{t}'\,\hat{b}\,G]\frac{e^{-jks}}{s}.$$

(b) Two-dimensional problems:

(23) $$d\bar{M} = \hat{z}\,dM_z + \hat{t}'\,dM_t,$$

(24) $$d\bar{E}(P) = \frac{-ke^{j\frac{\pi}{4}}}{\sqrt{8\pi k}} d\bar{M} \cdot [\hat{b}\,\hat{n}\,F + \hat{t}'\,\hat{b}\,G]\frac{e^{-jks}}{\sqrt{s}}$$

where $\hat{b} = \pm\,\hat{z}$.

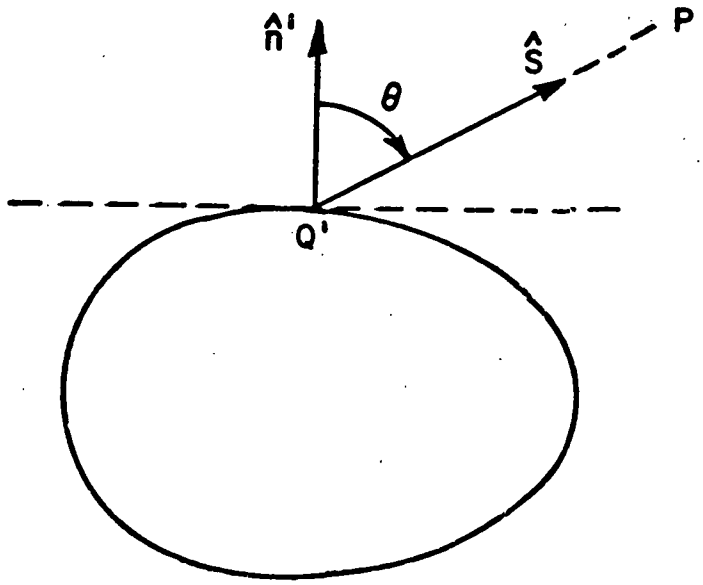

TABLE III

	F	G
1. $0 \leq \theta < \frac{\pi}{2} - \Delta$	F_1 as in Eq. (18a)	G_1 as in Eq. (18b)
2. $\frac{\pi}{2} - \Delta < \theta < \frac{\pi}{2} + \Delta$	F_2 as in Eq. (46); also Eq. (44)	G_2 as in Eq. (47); also Eqs. (44), (45)
3. $\frac{\pi}{2} + \Delta < \theta < \pi - \delta$	F_3 as in Eq. (12); also Table II and Eq. (36)	G_3 as in Eq. (14); also Table II and Eq. (35)

In application to two-dimensional problems

$$\sqrt{\frac{d\psi_o}{d\psi}} = 1$$

$\delta = 0$ unless an axial caustic of the diffracted rays is present in which case one employs Eq. (A-104) in the region $\pi - \delta < \theta \leq \pi$, where $\delta = (ka)^{-1/3}$ in this inequality and a is defined in Fig. 5A.

IV. PATTERN CALCULATIONS

In this Section, the expressions developed in the previous secions are employed to calculate the radiation from slots in cylinders, spheres, and spheroids. In dealing with the radiation from slots in perfectly-conducting cylinders, we formulate the problem in terms of its equivalent 2-dimensional representation; as noted earlier the radiation patterns of 2-dimensional, infinitely-long slots in cylinders are the same as those of the finite axial or circumferential slots when the patterns are calculated in the symmetry plane perpendicular to the axis of the cylinder. In the case of a slot in a perfectly-conducting spheroid, the slot dimensions are assumed to be infinitesimal; however this is not an essential limitation of the method, since an extended slot can be regarded as a continuous array of infinitesimal slots. Furthermore, these examples have been chosen so that the surface rays excited by the slot traverse geodesic paths with zero torsion;* this restriction is pointed out in the theoretical development of Section II. The radiation from slots in cylinders is treated first.

The expressions for F and G may be determined with the aid of Table III on page 25.

A. Radiation from Slots in Cylinders

A perfectly-conducting convex cylinder excited by a magnetic line source on its surface Q' is depicted in Fig. 8a. Two kinds of magnetic line sources M_z and M_t are considered; they are the equivalent sources of an infinitesimal axial slot, whose aperture electric field is in the circumferential and axial directions, respectively. Sources of this type have been discussed in Section II, Eqs. (20) and (21), and in Appendix I, part 3.

The GTD formulas for the far-zone field of this radiating system will be given in its shadow, transition and illuminated regions. The phase center of the field is chosen to be the origin O depicted in Fig. 8.

---

*The modifications required of the present formulation when the surface ray possesses torsion ($\hat{b}' \neq \hat{b}$) is not well understood at this time; however Eq. (15) may be applied formally to torsional surface rays by replacing $\hat{b}$ by $\hat{b}'$ in its first term. In a number of examples it has been found that the resulting accuracy is acceptable for practical purposes; however this can not be asserted for the general case without further work.

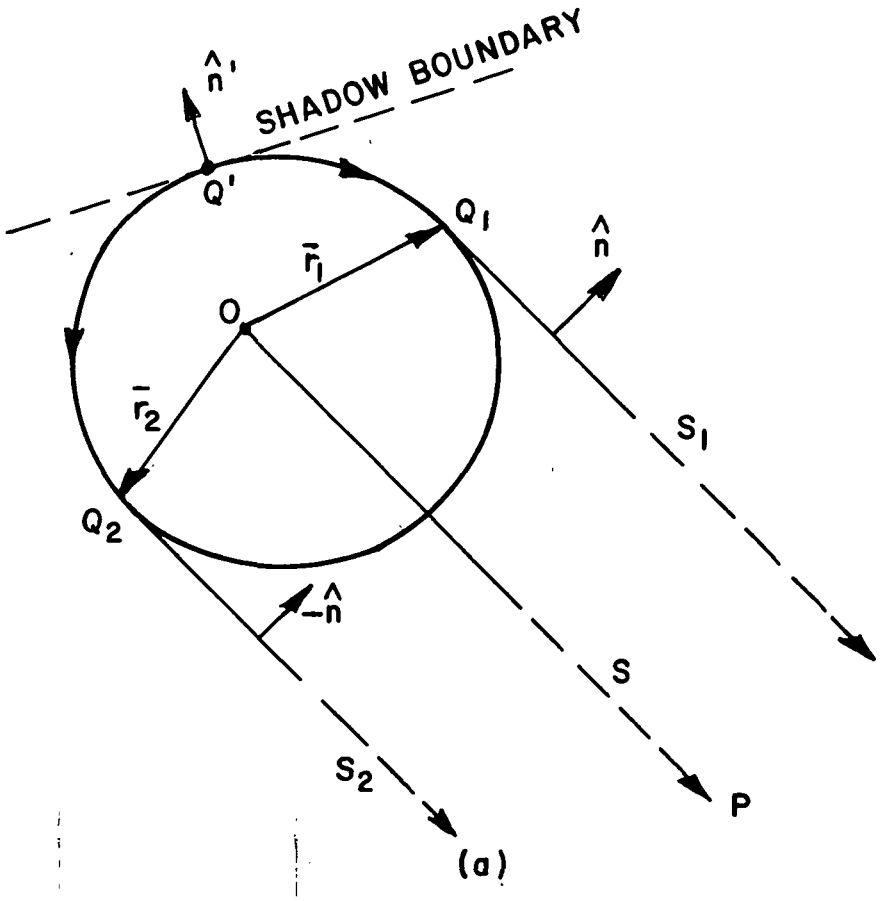

Fig. 8a. Ray geometry associated with a slot on a cylinder when P is in the shadow region.

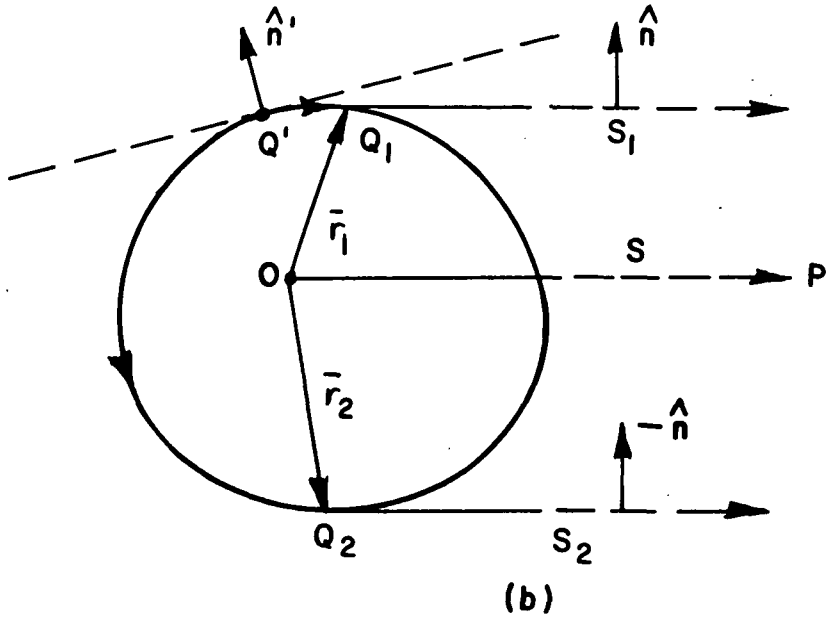

Fig. 8b. Ray geometry associated with a slot on a cylinder when P is in the transition region.

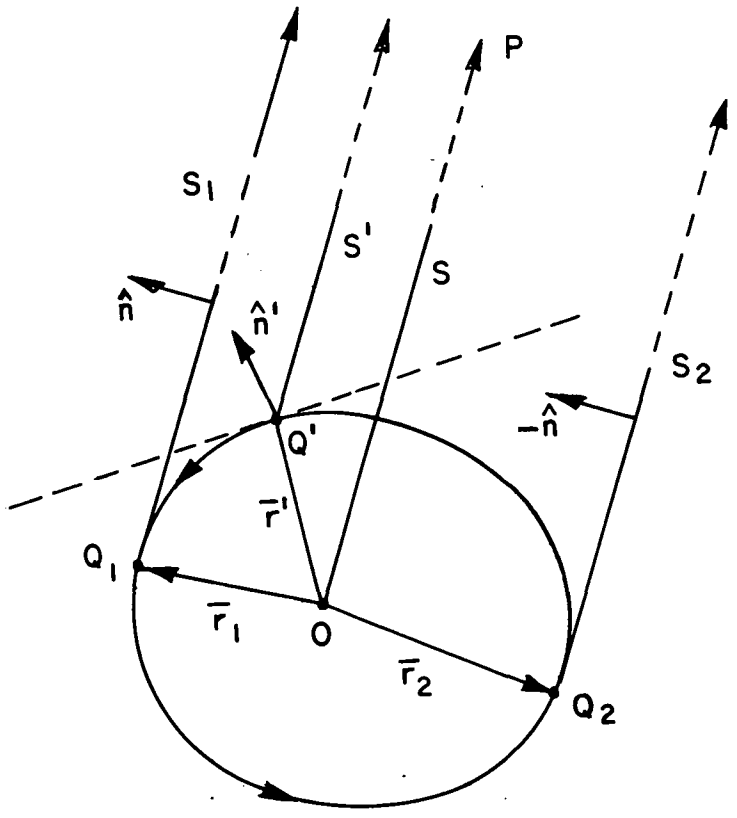

Fig. 8c. Ray geometry associated with a slot on a cylinder when P is in the illuminated region.

1. Deep shadow region

The contributions to the far-zone field at P come from the diffracted rays shed tangentially from the surface at Q_1 and Q_2 toward P, with the result that

$$(48) \quad E_n = \frac{-ke^{j\frac{\pi}{4}}}{2\sqrt{2\pi k}} M_z \left[F_3(Q',Q_1) e^{jk\bar{r}_1 \cdot \hat{s}} + F_3(Q',Q_2) e^{jk\bar{r}_2 \cdot \hat{s}} \right] \frac{e^{-jks}}{\sqrt{s}} ,$$

$$(49)\qquad E_z = \frac{-ke^{j\frac{\pi}{4}}}{2\sqrt{2\pi k}} M_t \left[G_3(Q',Q_1)e^{jk\bar{r}_1\cdot\hat{s}} + G_3(Q',Q_2)e^{jk\bar{r}_2\cdot\hat{s}} \right] \frac{e^{-jks}}{\sqrt{s}} ,$$

where the position vectors of Q_1 and Q_2 are $\bar{r}_1$ and $\bar{r}_2$, respectively, $\hat{s}$ is a unit vector in the direction of P, and the approximations

$$(50a)\qquad s_1 \simeq s - \bar{r}_1 \cdot \hat{s},$$

$$(50b)\qquad s_2 \simeq s - \bar{r}_2 \cdot \hat{s},$$

valid in the far zone have been employed.

The contribution from rays which encircle the cylinder one or more times before sheding tangentially from Q_1 or Q_2 can be neglected for all but the smallest cylinders with the hard boundary condition. There it can be taken into account by multiplying each term in the series of Eq. (12) by

$$(51)\qquad \sum_{n=0}^{\infty} e^{jknT - n\int_0^T \alpha_p^h(t')dt'} = \left(1 - e^{-jkT - \int_0^T \alpha_p^h(t')dt'} \right)^{-1}$$

in which T is the circumference of the cylinder. The contributions from the field of these multiply-encircling rays were found to be negligible in the calculated patterns shown in this report.

2a. Transition region (shadow part)

Again the contributions to the field at P come from the diffracted rays shed tangentially from the surface at Q_1 and Q_2 toward P, as shown in Fig. 8b, but in this case Q_1 is so close to Q' that the series of surface ray modes associated with this surface ray is poorly convergent and should be replaced by a Fock representation; hence

$$(52)\qquad E_n = \frac{-ke^{j\frac{\pi}{4}}}{2\sqrt{2\pi k}} M_z \left[F_2(Q',Q_1)e^{jk\bar{r}_1\cdot\hat{s}} + F_3(Q',Q_2)e^{jk\bar{r}_2\cdot\hat{s}} \right] \frac{e^{-jks}}{\sqrt{s}}$$

$$(53)\quad E_z = \frac{-ke^{j\frac{\pi}{4}}}{2\sqrt{2\pi k}} M_t \left[G_2(Q',Q_1) e^{jk\bar{r}_1\cdot\hat{s}} + G_3(Q',Q_2) e^{jk\bar{r}_2\cdot\hat{s}} \right] \frac{e^{-jks}}{\sqrt{s}}$$

2b. Transition region (illuminated part)

The contribution to the field at P comes from the ordinary diffracted ray shed tangentially from the surface at Q_1 toward P plus the contribution of the pseudo diffracted ray shed tangentially from Q_2, as shown in Fig. 8c. The far-zone fields of the two line sources are given by Eqs. (52) and (53), but it should be noted that t in G_2 is the arc length $Q'Q_1$, which is measured negatively, thus ξ too is negative.

3. Deep in the illuminated region

Referring to Fig. 8c the dominant contribution to the electric field at P comes from the geometrical optics field, which propagates along the direct, straight line path between Q' and P. For the two magnetic current line sources being considered this is

$$(54)\quad E_n^{g.o.} = \frac{-ke^{j\frac{\pi}{4}}}{\sqrt{2\pi k}} M_z e^{jk\bar{r}'\cdot\hat{s}} \frac{e^{-jks}}{\sqrt{s}} ,$$

$$(55)\quad E_z^{g.o.} = \frac{-ke^{j\frac{\pi}{4}}}{\sqrt{2\pi k}} M_t (\hat{n}'\cdot\hat{s}) e^{jk\bar{r}'\cdot\hat{s}} \frac{e^{-jks}}{\sqrt{s}} .$$

From the examples we have treated, it has been found that the geometrical optics field is so closely approximated by the field of the pseudo ray $Q'Q_1P$

$$(56)\quad E_n' = \frac{-ke^{j\frac{\pi}{4}}}{2\sqrt{2\pi k}} M_z F_2(Q',Q_1) e^{jk\bar{r}_1\cdot\hat{s}} \frac{e^{-jks}}{\sqrt{s}} ,$$

$$(57)\quad E_z' = \frac{-ke^{j\frac{\pi}{4}}}{2\sqrt{2\pi k}} M_t G_2(Q',Q_1) e^{jk\bar{r}_1\cdot\hat{s}} \frac{e^{-jks}}{\sqrt{s}} ,$$

that in many instances the above equations can be used in place of Eqs. (54) and (55) throughout the illuminated region.

In addition to the geometrical optics field there are much weaker contributions from the fields of the diffracted ray shed tangentially from Q_2 and the diffracted ray shed tangentially from Q_1 after traversing the surface in a clockwise direction from its source Q'. These diffracted ray contributions are significant only for the small cylinders excited by the M_z line source (the hard boundary case). In summary deep in the illuminated region

$$(58)\quad E_n = E_n^{g.o.} + \frac{-ke^{j\frac{\pi}{4}}}{2\sqrt{2\pi k}} M_z \left[F_3(Q',Q_2) e^{jk\bar{r}_2\cdot\hat{s}} + F_3(Q',Q_1) e^{jk\bar{r}_1\cdot\hat{s}} \right] \frac{e^{-jks}}{\sqrt{s}}$$

$$(59)\quad E_z = E_z^{g.o.} .$$

The patterns of axial slots in circular and elliptic cylinders have been calculated using the preceding formulas. In each case the electric field in the slot is circumferentially directed. Some patterns of an infinitesimally thin axial slot on circular cylinders of varying sizes are shown in Fig. 9. These patterns were calculated from Eqs. (48) and (52); it was unnecessary to use the geometrical optics representation deep in the illuminated region. In Fig. 9 the GTD patterns are compared with those calculated from the exact (eigenfunction) solution, and it is seen that for $ka > 3$ there are no significant differences between the patterns based on the GTD solution and the patterns calculated from the exact solution. Even for a cylinder as small as two wavelengths in circumference the error in the GTD pattern is seen to be small.

The pattern of a narrow axial slot in an elliptical cylinder is shown in Fig. 10. Eqs. (48), (52), and (56) were employed to calculate the GTD pattern; the finite width of the slot (0.34 wavelength) is taken into account by an array of 5 line sources in the aperture. This pattern is compared with a measured pattern of the same configuration in a plane perpendicular to the axis of the slot and cylinder[6]. The agreement between the measured and calculated values is good, since the discrepancy between the two halves of the measured pattern about its plane of symmetry is approximately the same as the differences between the measured and calculated values. This agreement is gratifying because it confirms the accuracy of the GTD solution in an example where the surface curvature is variable.

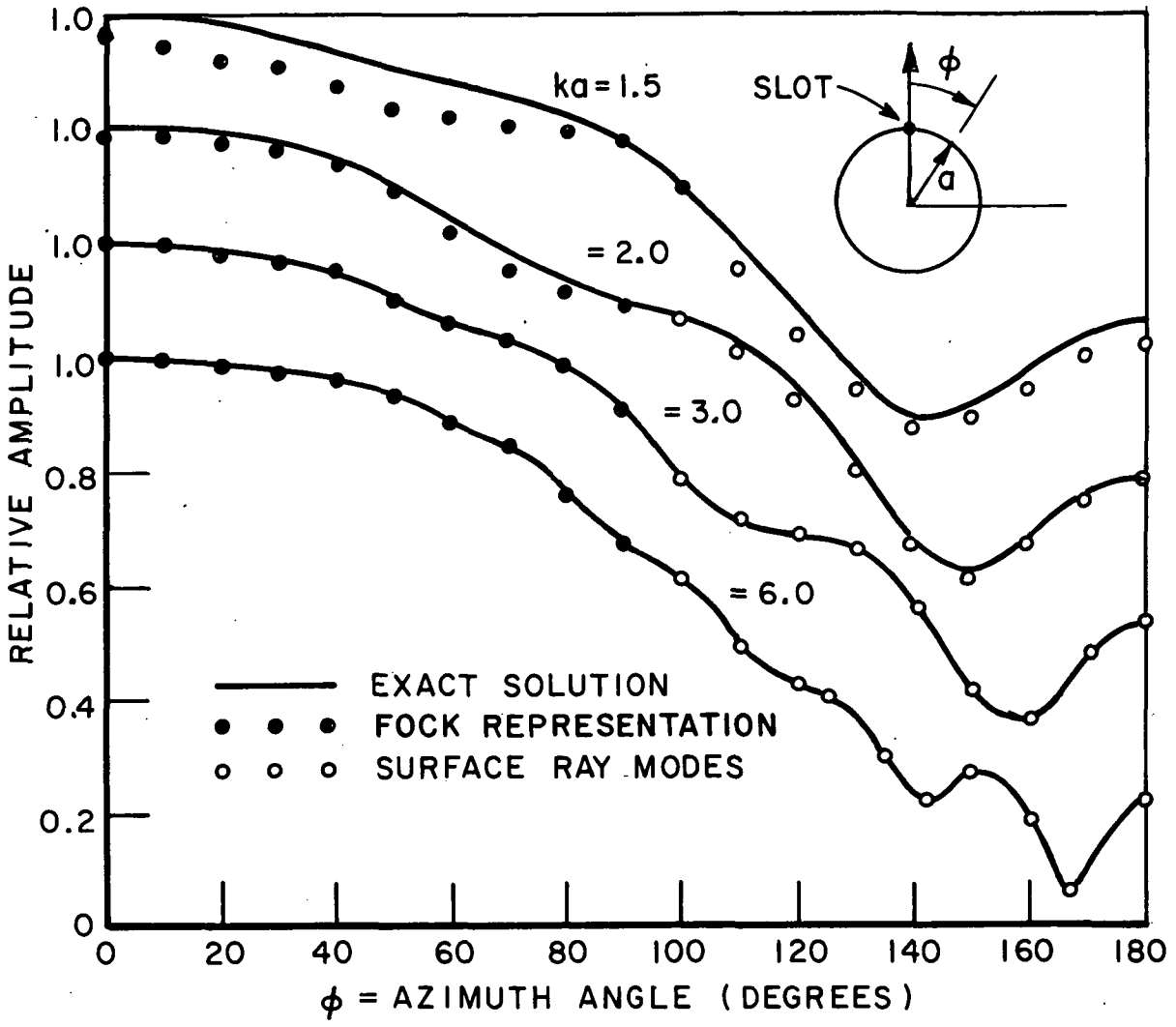

Fig. 9. Radiation patterns of a thin axial slot in a perfectly conducting circular cylinder.

The GTD patterns of infinitesimal axial slots at positions of maximum and minimum radii curvature on an elliptic cylinder are shown in Fig. 11. As one would expect, the level of the pattern in the shadow region is much lower for case A, where the elliptic cylinder tends to block the rearward directed radiation more.

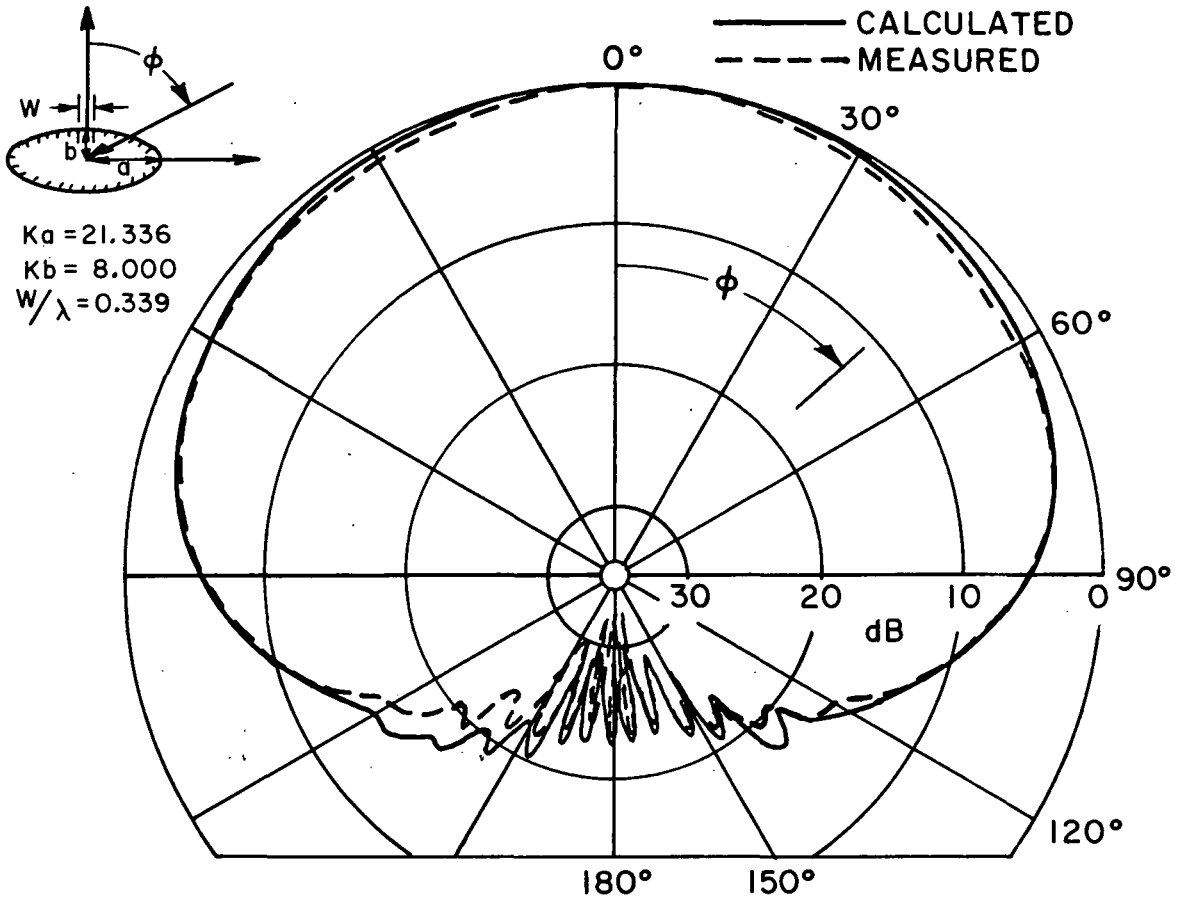

Fig. 10. Pattern of an axial slot on an elliptic cylinder.

B. Radiation From Slots in Spheres and Spheroids

In this section the pattern of an infinitesimal slot in a convex, finite surface of revolution is considered for the case where the slot is located on the axis of revolution. However, numerical results are presented for the spheroid and spherical surfaces only.

The equivalent source of an infinitesimal slot is the magnetic current moment $\bar{p}_m$ located at the position of the slot and directed parallel to its axis. A densely packed array of such magnetic current moments can serve as the equivalent source of slot of finite size; alternatively it could be represented as a continuous distribution as in Eq. (2).

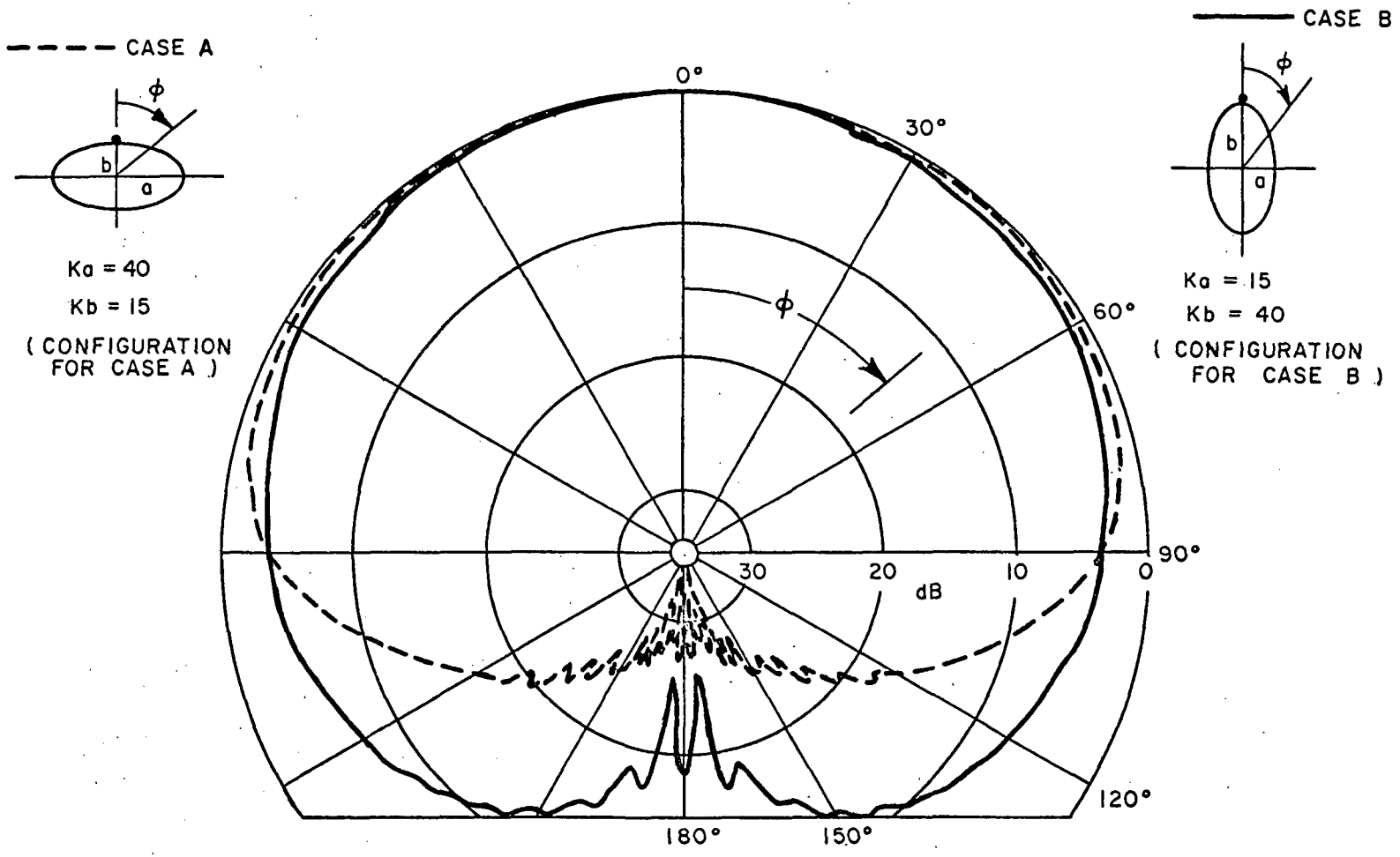

Fig. 11. Patterns of a narrow axial slot on an elliptic cylinder.

Now consider the radiation from an infinitesimal slot, with the magnetic current moment $\bar{p}_m = \hat{x}p_m$, as its equivalent source, located on the axis of a convex body of revolution at $z = z_o$, as shown in Fig. 12. From the symmetry of the problem, it follows that the radiation pattern can be completely specified in terms of the electric field pattern $E_{\parallel}(s,\theta)$ in the meridional plane parallel to the slot and the electric field pattern $E_{\perp}(s,\theta)$ in the meridional plane perpendicular to the slot; in other words, in terms of the H- and E-plane patterns.

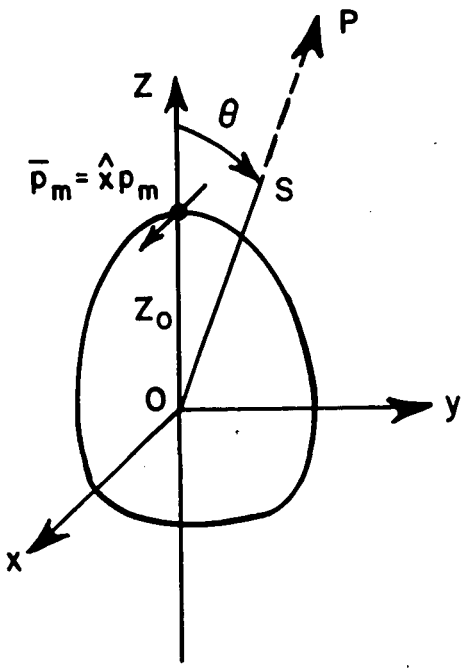

Fig. 12. Infinitesimal slot on the axis of a convex body of revolution.

Introducing the spherical coordinate system (s,θ,ϕ) in the far zone

$$\bar{E}(s,\theta,\phi) = -\hat{\phi}\, E_{\parallel}(s,\theta)\cos\phi - \hat{\theta}\, E_{\perp}(s,\theta)\sin\phi. \tag{60}$$

The GTD solution for the H- and E-plane patterns parallels the analysis carried out in the preceding section for the patterns of cylinders excited by the M_t and M_z magnetic line sources, respectively, with some differences:

1) the surface divergence $\sqrt{\frac{d\psi_o}{d\psi}}$ must be determined,

2) the product of C and the radial dependence of the far-zone field is $-jk\, e^{-jks}/4\pi s$,

3) there may be a caustic on the ray path,

4) there is a caustic of the diffracted rays at $\theta = \pi$ for the configuration shown in Fig. 12.

Figures 8(a,b,c) may be used to illustrate the pertinent ray trajectories for the body of revolution by considering the closed curve depicted in each figure to be the cross section of a body of revolution whose axis passes through the source point Q'.

1. Deep shadow region

$$E_{\parallel} = \frac{-jk}{4\pi} p_m \left[G_3(Q',Q_1) e^{jk\bar{r}_1\cdot\hat{s}} + jG_3(Q',Q_2) e^{jk\bar{r}_2\cdot\hat{s}} \right] \frac{e^{-jks}}{s} , \tag{61}$$

$$E_{\perp} = \frac{-jk}{4\pi} p_m \left[F_3(Q',Q_1) e^{jk\bar{r}_1\cdot\hat{s}} + jF_3(Q',Q_2) e^{jk\bar{r}_2\cdot\hat{s}} \right] \frac{e^{-jks}}{s} , \tag{62}$$

except in the region of the axial caustic of the diffracted rays, $\pi-\Delta<\theta<\pi$, where Eqs. (A-105), (A-106) are employed.

2. Transition region

$$E_{\parallel} = \frac{-jk}{4\pi} p_m \left[G_2(Q',Q_1) e^{jk\bar{r}_1\cdot\hat{s}} + jG_3(Q',Q_2) e^{jk\bar{r}_2\cdot\hat{s}} \right] \frac{e^{-jks}}{s} . \tag{63}$$

$E_{\perp}$ has the same form as $E_{\parallel}$ except that F replaces G. Also note the comments in the preceding section concerning the differences in the ray paths and the calculation of F and G resulting from the field point being in the shadow or illuminated parts of the transition region.

3. Deep in the illuminated region

$$E_{\parallel} = \frac{-jk}{4\pi} p_m \left[2(\hat{z}\cdot\hat{s}) e^{jk\bar{r}'\cdot\hat{s}} + jF_3(Q',Q_2) e^{jk\bar{r}_2\cdot\hat{s}} + jF_3(Q',Q_1) e^{jk\bar{r}_1\cdot\hat{s}} \right] \frac{e^{-jks}}{s} , \tag{64}$$

$$(65) \qquad E_{\perp} = \frac{-jk}{4\pi} p_m \left[2\, e^{jk\bar{r}'\cdot\hat{s}} + jG_3(Q',Q_2)e^{jk\bar{r}_2\cdot\hat{s}} + jG_3(Q',Q_1)e^{jk\bar{r}_1\cdot\hat{s}} \right] \frac{e}{s}^{-jk\hat{s}} ,$$

where $\bar{r}' = \hat{z}\, z_o$.

In evaluating F and G the surface divergence factor must be determined. For the axially-excited bodies of revolution under study it is a simple exercise of differential geometry to find $d\psi_o/d\psi$.

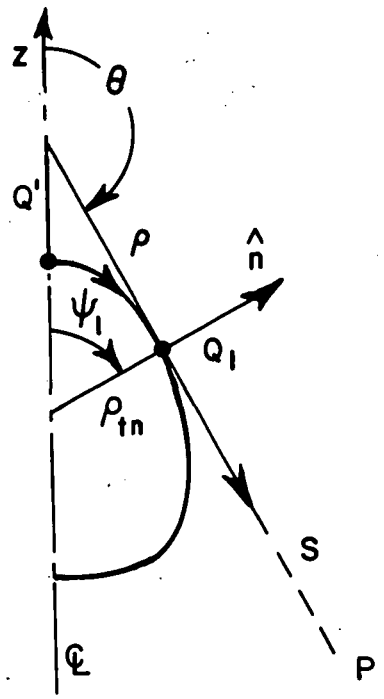

Fig. 13. Diffracted ray geometry.

Referring to Fig. 13

$$(66a) \qquad \frac{d\psi_o}{d\psi} = \frac{\rho}{\rho_{tn}\sin\psi_1} ,$$

where ρ_{tn} is the radius of curvature of the surface in the direction perpendicular to the ray, $\psi_1 = \cos^{-1}(\hat{n}\cdot\hat{z})$, and ρ is the caustic distance at the Q_1, where the diffracted ray sheds tangentially toward P. Since

$$\rho = \rho_{tn} \tan\psi_1, \tag{66b}$$

$$\frac{d\psi_o}{d\psi} = \frac{1}{\cos\psi_1} . \tag{66c}$$

$E_{\parallel}$ and $E_{\perp}$ given in Eqs. (61) through (65) may be substituted into Eq. (60) to calculate the far-zone field at any aspect. The preceding expression for $E_{\parallel}$ and $E_{\perp}$ have been used to calculate the patterns of infinitesimal slots on perfectly-conducting spheres and spheroids. In Figs. 14 and 15 the patterns in meridional planes parallel and perpendicular to an infinitesimal slot are shown in Figs. 14 and 15, where they are compared with exact values calculated by King and Wu[12]. Although King and Wu actually calculated the currents on a perfectly-conducting sphere illuminated by a plane wave, their results can be compared directly with ours through the reciprocity principle. The GTD patterns are seen to agree very well with the rigorously calculated patterns; as a matter of fact in Fig. 15, they are seen to be in better agreement with these patterns, than a pattern calculated from a formal asymptotic solution given by Belkina[4].

The GTD patterns of axially-positioned, infinitesimal slots on oblate and prolate spheroids are shown in Figs. 16 through 19. No rigorously calculated or measured patterns were available for comparison in these cases; however, the pattern for each spheroid is compared with the pattern of a slot on sphere with the same radius of curvature as the spheroid at its axis of revolution, where the slot is positioned. It is seen that spheres and spheroids with the same radii of curvature at their slot positions have essentially the same patterns in the illuminated and transition regions; the significant differences occur only in the deep shadow regions of their patterns. Considering the nature of the GTD solution described in Sections II and III, this result is not entirely unexpected.

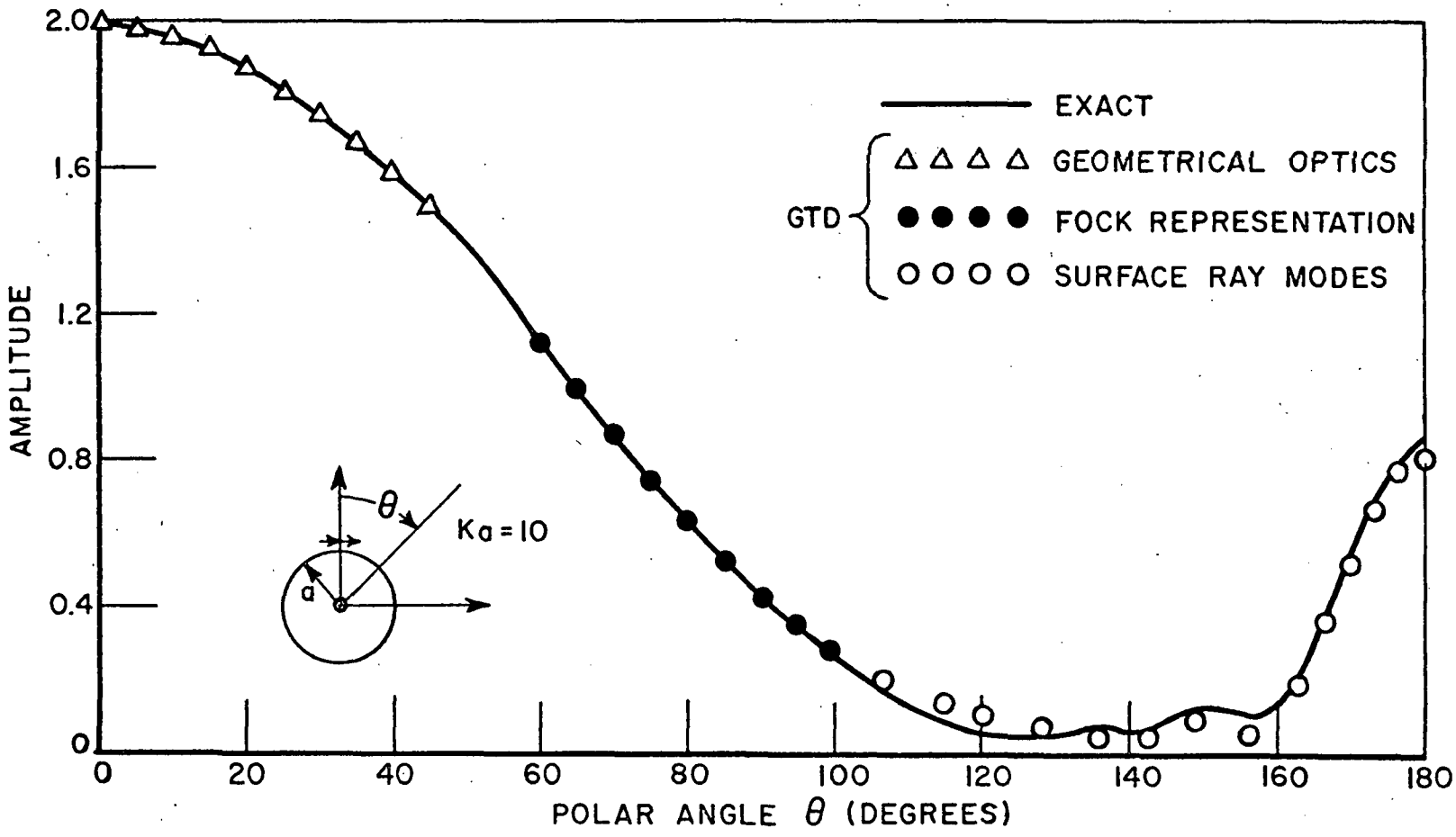

Fig. 14. Pattern of an infinitesimal slot on a sphere in a plane parallel to the slot.

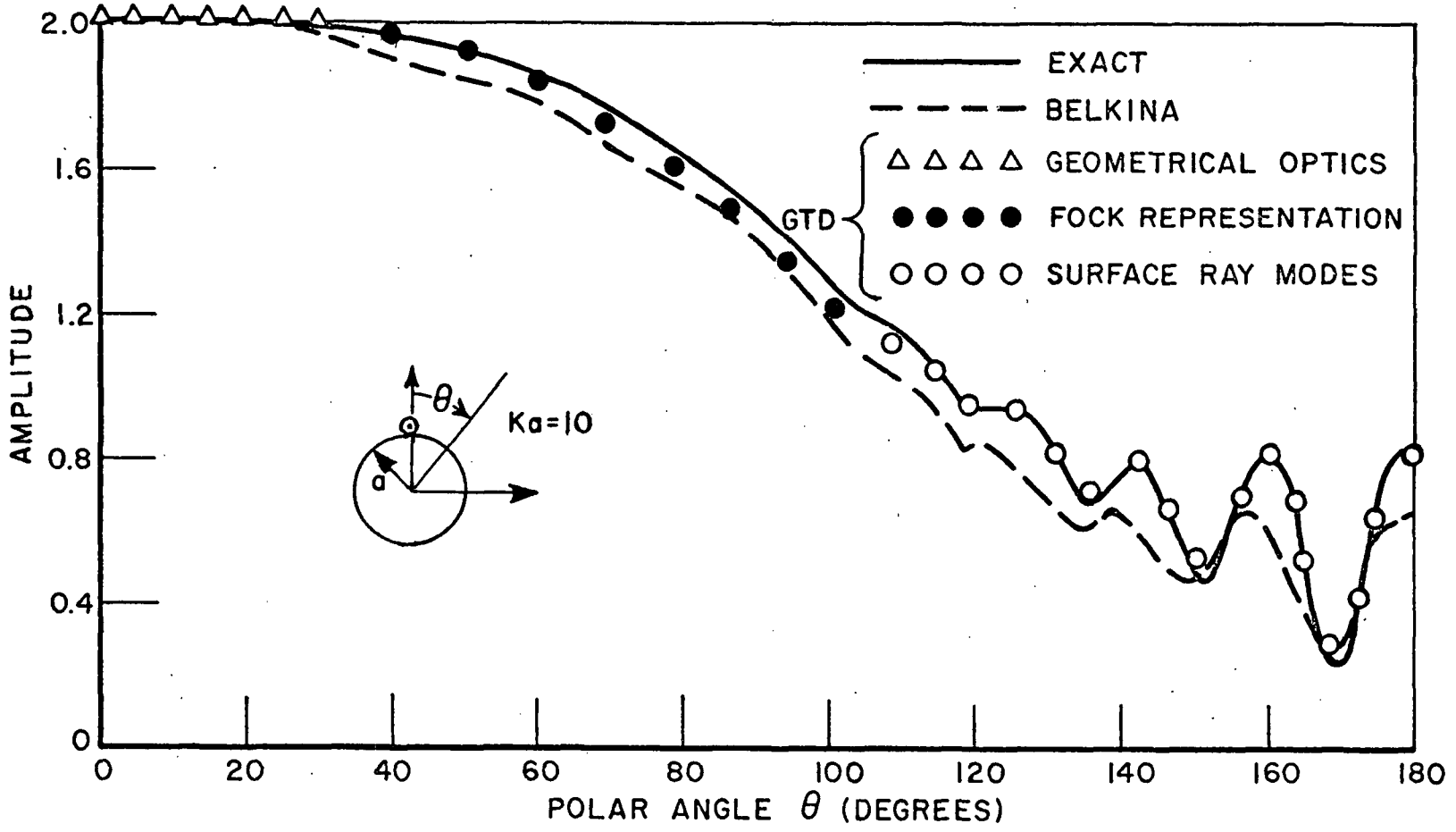

Fig. 15. Pattern of an infinitesimal slot on a sphere in a plane perpendicular to the slot.

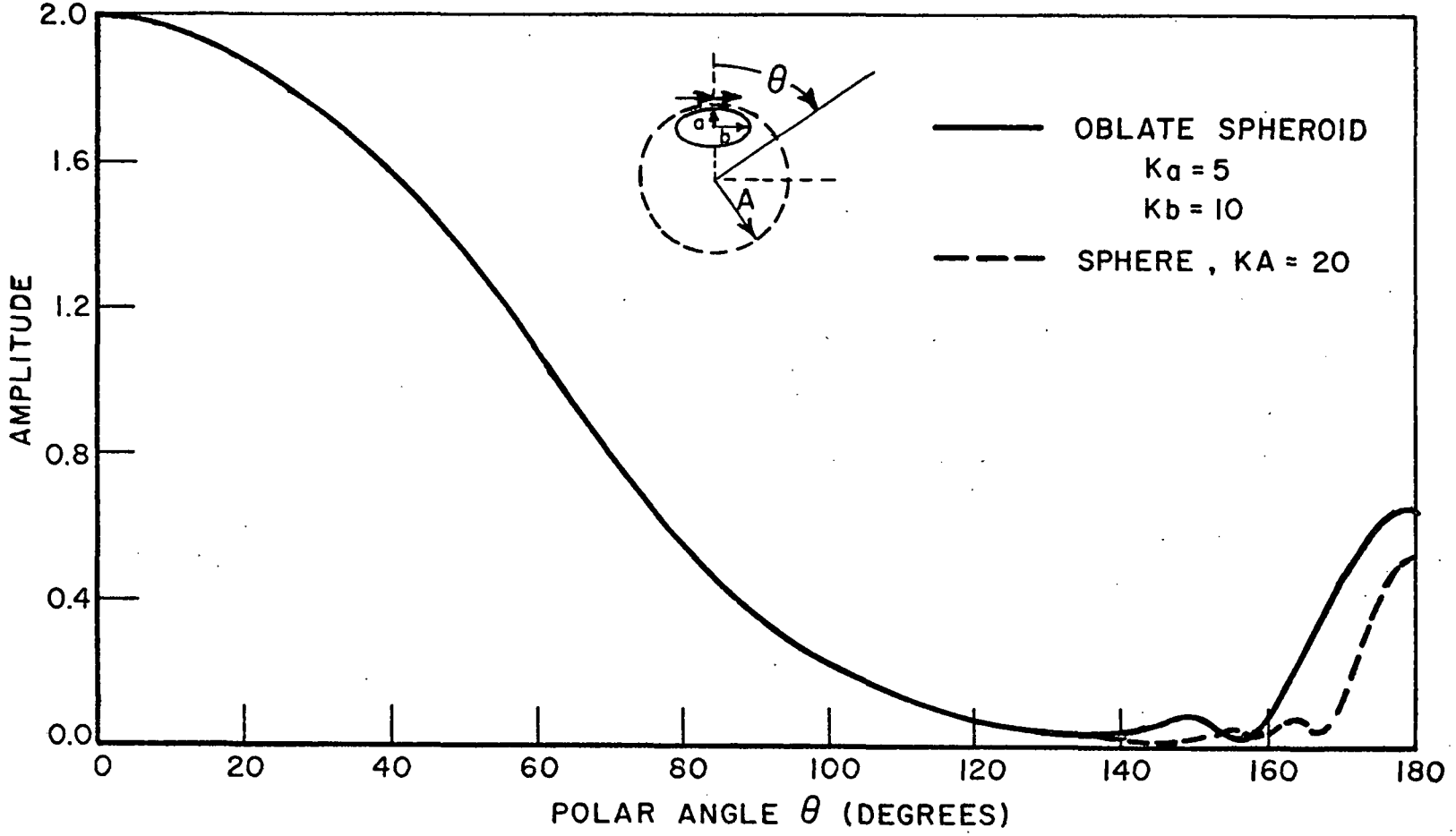

Fig. 16. Pattern in plane ∥ slot.

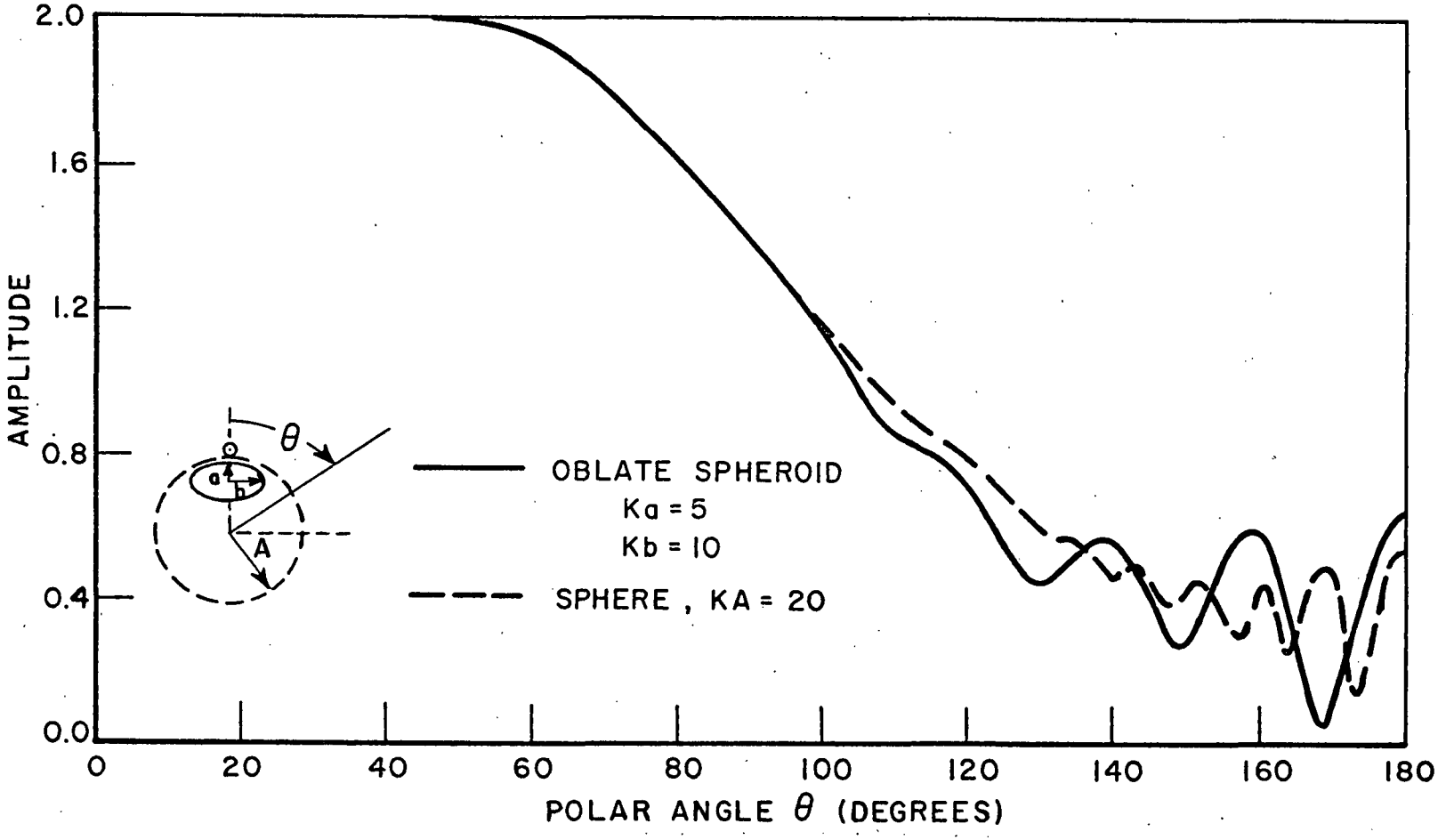

Fig. 17. Pattern in plane ⊥ slot.

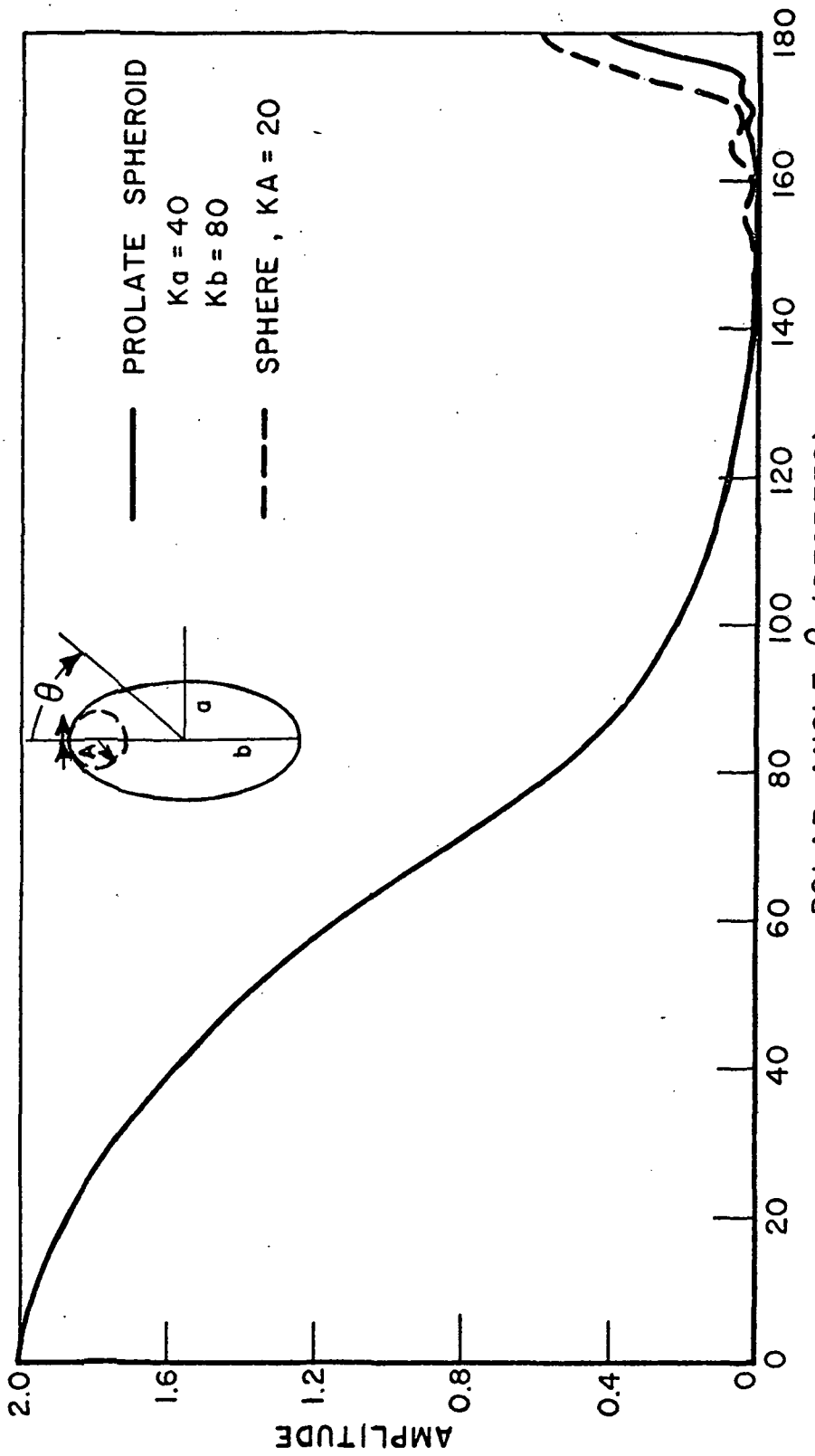

Fig. 18. Pattern in plane ∥ slot.

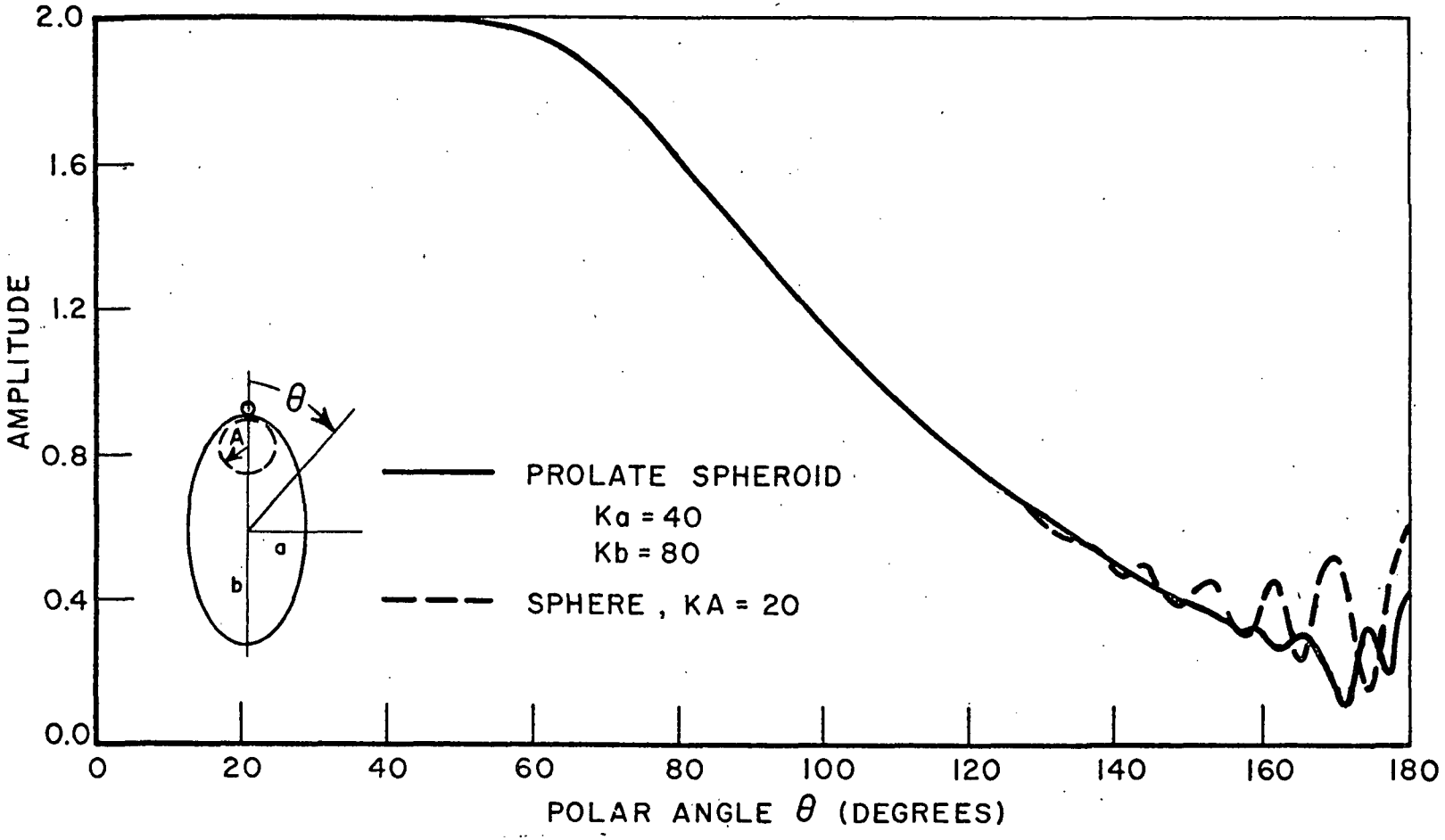

Fig. 19. Pattern in plane ⊥ slot.

V. CONCLUSIONS

Keller's geometrical theory of diffraction has been extended so that the radiation from apertures (slots) in perfectly-conducting smooth curved surfaces can be treated. Configurations of this type are of interest in the design of flush-mounted antennas for aircraft and spacecraft. In extending the GTD, a new parameter has been introduced, the launching coefficient, which relates the amplitudes and phases of the surface ray modes to the equivalent source in the aperture. This extension of the GTD has been successfully supplemented in the transition region and at axial caustics so that the pattern can be calculated at all aspects.

Although the present formulation is restricted to torsionless surface rays, it can be formally applied to surface rays with torsion, see Reference [25]. Examples considered in this reference suggest that moderate torsion does not result in excessive error in the pattern calculation. The propagation along surface rays with torsion is currently under study.

Although the calculation of far-zone fields is described here, the method can be applied to calculate near-zone fields without any additional assumptions. Furthermore, by introducing a second new parameter, the attachment coefficient, the GTD can be extended to determine the tangential magnetic field at the perfectly-conducting surface, so that the mutual coupling between apertures can be calculated; this will be the subject of a future report.

APPENDIX I
DETERMINATION OF THE LAUNCHING COEFFICIENTS

The canonical problems chosen to find the launching coefficients are the radiation from a magnetic current moment on the surface of a perfectly-conducting sphere and the radiation from two types of magnetic line sources on the surface of a perfectly-conducting cylinder. In the case of the first problem the asymptotic solutions for the E- and H-plane patterns are sufficient to determine the launching coefficients for the hard and soft boundary conditons.

The radiation from a magnetic current moment on the surface of a perfectly-conducting sphere may be formulated conveniently in terms of a dyadic Green's function. The properties of dyadic Green's functions have been described by C.T. Tai in Reference [19]; the dyadic Green's functions for simple geometries, including the sphere are also given in this reference.

Consider a perfectly-conducting sphere of radius a, whose center is at the origin of a spherical coordinate system as shown in Fig. 1A.

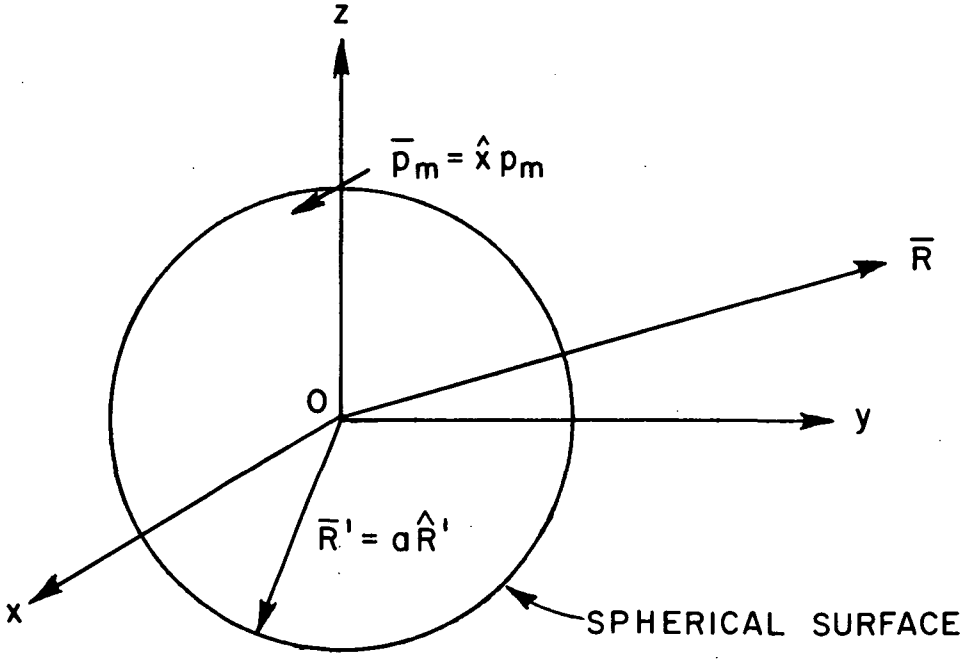

Fig. 1A. Infinitesimal slot on a sphere.

The electric field of the magnetic current moment $\bar{p}_m = \hat{x}\, p_m$ positioned on its surface at $\bar{R}' = a\hat{z}$, i.e., $R' = a$, $\theta = 0$, is

$$\text{(A-1)} \qquad \bar{E}(\bar{R}) = p_m \hat{x} \cdot [\nabla' \times \bar{\bar{G}}_1 (\bar{R}', \bar{R})]\Big|_{\bar{R}'=a\hat{z}}$$

where

$$\text{(A-2)} \qquad \bar{\bar{G}}_1(\bar{R}', \bar{R}) = \bar{\bar{G}}_0(\bar{R}', \bar{R}) + \bar{\bar{G}}_{1s}(\bar{R}', \bar{R}),$$

$$\text{(A-3)} \qquad G_0(\bar{R}', \bar{R}) = -\frac{jk}{4\pi} \sum_{n=1}^{\infty} \sum_{m=0}^{n} (2-\delta_0) \frac{2n+1}{n(n+1)} \frac{(n-m)!}{(n+m)!} \times$$

$$\times \left[\bar{M}'_{\substack{e_{mn} \\ o_{mn}}}(k)\, \bar{M}^{(2)}_{\substack{e_{mn} \\ o_{mn}}}(k) + \bar{N}'_{\substack{e_{mn} \\ o_{mn}}}(k)\, \bar{N}^{(2)}_{\substack{e_{mn} \\ o_{mn}}}(k) \right],$$

$$\text{(A-4)} \qquad G_{1s}(\bar{R}', \bar{R}) = -\frac{jk}{4\pi} \sum_{n=1}^{\infty} \sum_{m=0}^{n} (2-\delta_0) \frac{2n+1}{n(n+1)} \frac{(n-m)!}{(n+m)!} \times$$

$$\times \left[a_{\substack{e_n \\ o_n}}\, \bar{M}^{(2)'}_{\substack{e_{mn} \\ o_{mn}}}(k)\, \bar{M}^{(2)}_{\substack{e_{mn} \\ o_{mn}}}(k) + b_{\substack{e_n \\ o_n}}\, \bar{N}^{(2)'}_{\substack{e_{mn} \\ o_{mn}}}(k)\, \bar{N}^{(2)}_{\substack{e_{mn} \\ o_{mn}}}(k) \right],$$

$$\text{(A-5a)} \qquad a_{\substack{e_n \\ o_n}} = -\, j_n(ka)/h_n^{(2)}(ka),$$

$$\text{(A-5b)} \qquad b_{\substack{e_n \\ o_n}} = -\, [\rho_a j_n(\rho_a)]'/[\rho_a h_n^{(2)}(\rho_a)]',$$

$$\text{(A-5c)} \qquad \rho_a = ka,$$

$$\text{(A-5d)} \qquad \delta_0 = \begin{cases} 1, & m=0 \\ 0, & m\neq 0, \end{cases}$$

(A-5e) $R > R' = a.$

The time convention used by Tai is $e^{-i\omega t}$ whereas our time convention is $ej\omega t$; hence the superscript (1) in his formulas must be replaced by (2), which denotes a spherical Hankel function of the second kind, also i in his formulas must be replaced by -j in ours. The spherical vector wave functions $\overline{M}_{\substack{e\\o}mn}$ and $\overline{N}_{\substack{e\\o}mn}$ are given in Chapter 11 of Reference [19].

It is readily shown that

$$(A\text{-}6a) \qquad \hat{x} \cdot \overline{N}'_{\substack{e\\o}mn}(k) = \hat{x} \cdot \overline{N}'_{e1n}(k) = -\frac{1}{2} n(n+1) \frac{[\rho_a j_n'(\rho_a)]}{\rho_a} ,$$

and

$$(A\text{-}6b) \qquad \hat{x} \cdot \overline{M}'_{\substack{e\\o}mn}(k) = \hat{x} \cdot \overline{M}'_{o1n}(k) = \frac{1}{2} n(n+1)\, j_n(\rho_a) .$$

Substituting the above into Eq. (A-1)

$$(A\text{-}7) \qquad \overline{E}(\overline{R}) = \frac{jk^2 p_m}{4\pi} \sum_{n=1}^{\infty} \frac{2n+1}{n(n+1)} \left[\left\{ \frac{[\rho_a j_n(\rho_a)]'}{\rho_a} - \frac{j_n(\rho_a)}{h_n^{(2)}(\rho_a)} \frac{[\rho_a h_n^{(2)}(\rho_a)]'}{\rho_a} \right\} \overline{M}_{e1n}^{(2)}(k) - \left\{ j_n(\rho_a) - \frac{[\rho_a j_n(\rho_a)]'}{[\rho_a h_n^{(2)}(\rho_a)]'} h_n^{(2)}(\rho_a) \right\} \overline{N}_{o1n}^{(2)}(k) \right] .$$

In the far-zone the vector wave functions may be approximated by

$$(A\text{-}8a) \qquad \overline{M}_{e1n}^{(2)} = j^{(n+1)} \frac{e^{-jkR}}{kR} \overline{m}_{e1n}(\theta,\phi),$$

$$(A\text{-}8b) \qquad \overline{N}_{o1n}^{(2)} = j^{n} \frac{e^{-jkR}}{kR} \hat{R} x \overline{m}_{o1n}(\theta,\phi),$$

in which

$$\text{(A-9a)} \qquad \bar{m}_{eln} = -\frac{P_n^1(\cos\theta)}{\sin\theta}\sin\phi\hat{\theta} - \frac{dP_n^1(\cos\theta)}{d\theta}\cos\phi\hat{\phi},$$

$$\text{(A-9b)} \qquad \hat{R}X\,\bar{m}_{oln} = \frac{dP_n^1(\cos\theta)}{d\theta}\sin\phi\hat{\theta} + \frac{P_n^1(\cos\theta)}{\sin\theta}\cos\phi\hat{\phi}\ .$$

Employing Eqs. (A-8) and (A-9) in Eq. (A-7), the electric field in the far-zone is

$$\text{(A-10)} \qquad \bar{E}(\bar{R}) = \frac{jk^2 p_m}{4\pi}\frac{e^{-jkR}}{kR}\sum_{n=1}^{\infty}(j)^n\frac{2n+1}{n(n+1)}\left[\left\{\frac{\hat{J}_n'(ka)}{ka} - \frac{\hat{J}_n(ka)}{\hat{H}_n^{(2)}(ka)}\frac{\hat{H}_n^{(2)'}(ka)}{ka}\right\} j\,\bar{m}_{eln}(\theta,\phi) - \left\{\frac{\hat{J}_n(ka)}{ka} - \frac{\hat{J}_n'(ka)}{H_n^{(2)'}(ka)}\frac{\hat{H}_n^{(2)}(ka)}{ka}\right\}\hat{R}\times\bar{m}_{oln}(\theta,\phi)\right],$$

where

$$\text{(A-11a)} \qquad \hat{Z}_n(kr) = \sqrt{\frac{\pi kr}{2}}\,Z_{n+\frac{1}{2}}(kr),$$

$$\text{(A-11b)} \qquad \hat{Z}_n'(kr) = kr\,\tilde{Q}\,Z_{n+\frac{1}{2}}(kr),$$

in which $Z_{n+1/2}(kr)$ is a solution of Bessel's differential equation of order $n+1/2$ and $\tilde{Q}$ is an operator defined by

$$\text{(A-12)} \qquad \tilde{Q} = \sqrt{\frac{\pi}{2kr}}\left(\frac{1}{r}\frac{\partial}{\partial r} + \frac{1}{2kr}\right).$$

Substituting Eqs. (A-11) and (A-12) into Eq. (A-10)

$$(A\text{-}13)\qquad \overline{E}(\overline{R}) \sim \frac{jk^2 p_m}{4\pi}\,\frac{e^{-jkR}}{kR}\sum_{n=1}^{\infty}(j)^n\,\frac{2n+1}{n(n+1)}$$

$$\left[j\left\{ \tilde{Q}\, J_{n+\frac{1}{2}}(ka) - \frac{J_{n+\frac{1}{2}}(ka)}{H^{(2)}_{n+\frac{1}{2}}(ka)}\,\tilde{Q}\, H^{(2)}_{n+\frac{1}{2}}(ka)\right\}\frac{dP_n^1(\cos\theta)}{d\theta}\cos\phi\hat{\phi} + \right.$$

$$\left. + \sqrt{\frac{\pi}{2ka}}\left\{ J_{n+\frac{1}{2}}(ka) - \frac{\tilde{Q}\, J_{n+\frac{1}{2}}(ka)}{\tilde{Q}\, H^{(2)}_{n+\frac{1}{2}}(ka)}\, H^{(2)}_{n+\frac{1}{2}}(ka)\right\}\frac{dP_n^1(\cos\theta)}{d\theta}\sin\phi\hat{\theta}\right],$$

where terms involving $\frac{P_n^1(\cos\theta)}{ka\,\sin\theta}$ have been neglected, because the solution for $ka\sin\theta \gg 1$ is of interest.

The relationships

$$(A\text{-}14a)\qquad \frac{d}{d\theta}\,P_n^1(\cos\theta) = (-1)^{-n}\,n(n+1)\,\frac{d}{d\theta}\,P_n^{-1}(-\cos\theta)$$

and

$$(A\text{-}14b)\qquad J_{n+\frac{1}{2}}(kr) = \frac{1}{2}\left[H^{(1)}_{n+\frac{1}{2}}(kr) + H^{(2)}_{n+\frac{1}{2}}(kr)\right]$$

are employed in the development to follow..

1. H-plane ($\phi = 0$) Soft EM boundary

Using Eq. (A-14), it follows from Eq. (A-13) that

$$(A\text{-}15)\qquad \overline{E} \sim -\hat{\phi}\ \frac{k^2 p_m}{4}\ \frac{e^{-jkR}}{kR}\ \sum_{n=1}^{\infty} (-j)^n \left(\frac{2n+1}{2}\right) \left\{ \tilde{Q}\ H^{(1)}_{n+\frac{1}{2}}(ka) - \right.$$

$$\left. - \frac{H^{(1)}_{n+\frac{1}{2}}(ka)}{H^{(2)}_{n+\frac{1}{2}}(ka)}\ \tilde{Q}\ H^{(2)}_{n+\frac{1}{2}}(ka) \right\} \frac{dP_n^{-1}(-\cos\theta)}{d\theta} \quad .$$

The Watson transformation facilitates the asymptotic approximation of Eq. (A-15) and its transformation to a ray optical form suitable for calculating the field in the shadow region. Accessible descriptions of the method are given in References [16,20]. Applying the Watson transformation to Eq. (A-15) and evaluating the resulting integral by the residues of its integrand at $\nu = \nu_p$,

$$(A\text{-}16)\qquad E_\phi \sim -\frac{kp_m}{2}\ \frac{e^{-jkR}}{R}\ \sum_{p=1}^{\infty} \frac{e^{-j\nu_p \frac{\pi}{2}}\ e^{-j\frac{\pi}{4}}}{1+e^{-j2\nu_p}} \cdot \nu_p \left\{ - \frac{H^{(1)}_{\nu_p}(ka)}{\left\{\frac{\partial}{\partial\nu} H^{(2)}_{\nu}(ka)\right\}_{\nu_p}} \cdot \right.$$

$$\left. \cdot\ \tilde{Q}\ H^{(2)}_{\nu_p}(ka) \right\} \frac{\partial P^{-1}_{\nu_p - 1/2}(-\cos\theta)}{\partial\theta}$$

with ν_p being the complex orders for which $H^{(2)}_{\nu_p}(ka) = 0$, $p = 1,2,3\cdots$. For large ka

$$(A\text{-}17)\qquad \nu_p = ka + \left(\frac{ka}{2}\right)^{1/3} q_p\ e^{-j\frac{\pi}{3}}$$

$$= ka \left[1 + \frac{1}{2} \left(\frac{2}{ka}\right)^{2/3} q_p\ e^{-j\frac{\pi}{3}} \right]$$

to first order, since q_p is real (see Table I), the imaginary part of $\nu_p$mis negative and proportional to $(ka/2)^{1/3}$. It is assumed here that ka is sufficiently large that

$$\left(1 + e^{-j2\nu_p \pi}\right)^{-1}$$

can be replaced by one. Furthermore when $ka \sin\theta >> 1$,

$$(A\text{-}18)\quad \nu_p \frac{\partial P^{-1}_{\nu_p - 1/2}(-\cos)}{\partial\theta} \sim \sqrt{\frac{2}{\pi ka \sin\theta}}\ \frac{e^{j\nu_p\pi}\, e^{-j\frac{\pi}{4}}}{2}\left[e^{-j\nu_p\theta} + je^{-j\nu_p(2\pi-\theta)}\right] \cdot$$

$$\cdot\ ka\left[1 + \frac{1}{4}e^{-j\frac{\pi}{3}} q_p \left(\frac{2}{ka}\right)^{2/3}\right]$$

From Keller and Levy[15]

$$(A\text{-}19)\quad \frac{H^{(1)}_{\nu_p}(ka)}{\frac{\partial}{\partial\nu} H^{(2)}_{\nu_p}(ka)} = -\left(\frac{jk}{2\pi}\right)^{1/2}(D^s_{op})^2,$$

with D^s_{op} the soft diffraction coefficient, which is given by Eq. (27) after asymptotically approximating the Hankel functions to first order. Also

$$(A\text{-}20)\quad \tilde{Q}\, H^{(2)}_{\nu_p}(ka) = \sqrt{\frac{\pi}{2ka}}\, H^{(2)'}_{\nu_p}(ka),$$

since $H^{(2)}_{\nu_p}(ka) = 0$.

If we let

$$(A\text{-}21a,b)\quad \psi_1 = \theta - \frac{\pi}{2} \text{ and } \psi_2 = \frac{3\pi}{2} - \theta$$

and make use of Eqs. (A-18), (A-19) and (A-20), Eq. (A-16) becomes

$$(A\text{-}22)\quad E_\phi \sim -\frac{jk}{4\pi}\frac{p_m}{\sin\theta}\sum_{p=1}^{\infty}\left\{-\pi\left(\frac{jk}{2\pi}\right)^{1/2} H^{(2)'}_{\nu_p}(ka) D^s_p\right\}$$

$$\times\left[e^{-j\nu_p\psi_1} + j\, e^{-j\nu_p\psi_2}\right] D^s_p \frac{e^{jkR}}{R},$$

which is an asymptotic approximation for the electric field in the shadow region of the H-plane for $\theta < \pi$. The D_p^s are the soft EM diffraction coefficients for the sphere given in Table I.

Next let us use the GTD method described in Section I to find E_ϕ. By comparing the resulting expression with the asymptotic approximation, the launching coefficients and the constant C can be found. Consider the field point P in the shadow region of the H-plane; according to Keller's generalized Fermat's principle, two surface rays emanate from the magnetic current moment at $\bar{R}' = az$ and traverse paths t_1 and t_2 along merideans to Q_1 and Q_2, where they tangentially shed the diffracted rays 1 and 2 toward P, as shown in Fig. 2-A. Thus the total far-zone electric field at P is the sum of the fields contributed by diffracted rays 1 and 2. It is assumed that ka is sufficiently large that the contribution from the surface ray which encircles the sphere one or more times before shedding a diffracted ray toward P can be neglected. This is consistent with replacing

$$(1 + e^{j2\nu_p \pi})^{-1}$$

by one in the asymptotic approximation. Since $\bar{p}_m \cdot \hat{t}' = p_m$ and $\bar{p}_m \cdot \hat{b} = 0$, one obtains

$$E_\phi = Cp_m G_1 \frac{e^{-jks_1}}{s_1} + Cp_m G_2 \frac{e^{-jks_2}}{s_2} \qquad \text{(A-23)}$$

with

$$t_1 = a(\theta - \tfrac{\pi}{2}) = a\psi_1, \qquad \text{(A-24a)}$$

$$t_2 = a(\tfrac{3\pi}{2} - \theta) \doteq a\psi_2, \qquad \text{(A-24b)}$$

$$s_1 = s_2 = R, \qquad \text{(A-24c)}$$

and

$$\sqrt{\frac{d\psi_o}{d\psi}} = \frac{1}{\sqrt{\sin\theta}} \quad \text{for both } Q_1 \text{ and } Q_2, \qquad \text{(A-24d)}$$

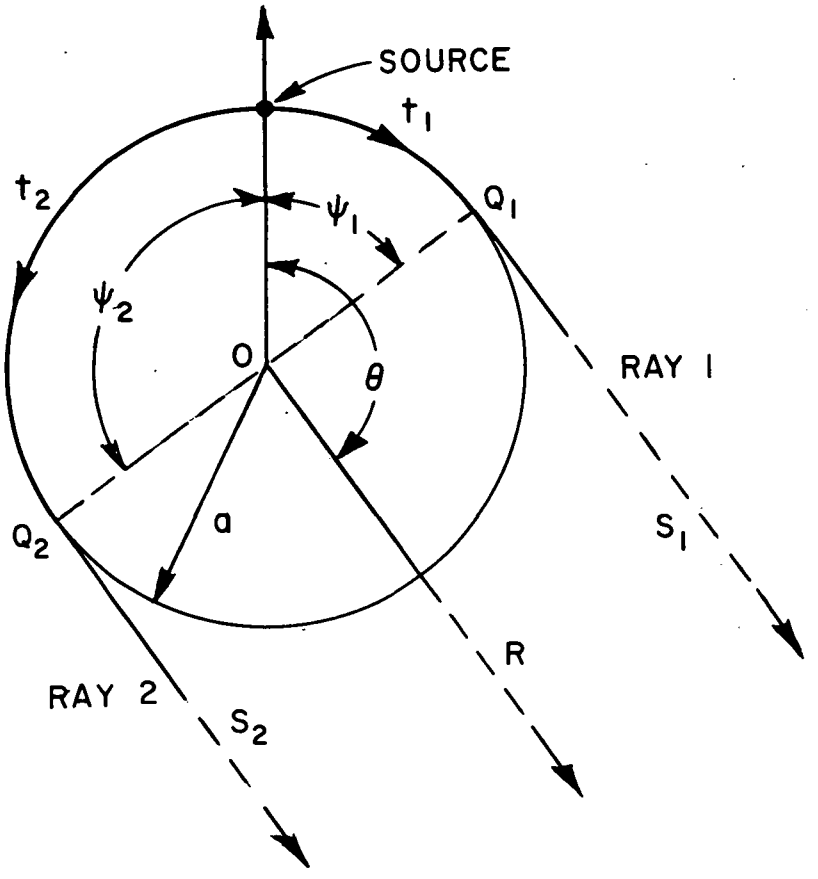

Fig. 2A. Ray geometry associated with a source on a cylinder or sphere.

Upon using Eq. (14),

$$(A\text{-}25) \qquad E_\phi = \frac{Cp_m}{\sqrt{\sin\theta}} \sum_{p=1}^{\infty} L_p^s D_p^s \left[e^{-(jk+\alpha_p^s)a\psi_1} + je^{-(jk+\alpha_p^s)a\psi_2} \right] \frac{e^{-jkR}}{R}$$

where the factor j has been inserted to account for the phase jump of $\pi/2$ resulting from the caustic on ray path 2. This is the GTD expression for E_ϕ; comparing it with the asymptotic approximation in Eq. (A-22)

$$(A\text{-}26) \qquad C = -\frac{jk}{4\pi},$$

$$(A\text{-}27) \qquad L_p^s = -\pi \left(\frac{jk}{2\pi}\right)^{1/2} H_{\nu_p}^{(2)'}(ka) D_p^s,$$

$$(A\text{-}28) \qquad \nu_p = ka - j\alpha_p^s a.$$

The constant C is chosen to make Eq. (15) consistent with Eq. (17). The formula for α_p^s has been obtained previously from other canonical problems, (see Table I). Since $\nu_p \approx ka$ and $ka \gg 1$, $H_{\nu_p}^{(2)'}(ka)$ may be approximated asymptotically in terms of an Airy function[9]

$$(A\text{-}29) \qquad H_{\nu_p}^{(2)'}(ka) \sim -2e^{-j\frac{\pi}{3}} \left(\frac{2}{ka}\right)^{2/3} Ai'(-q_p) \left\{ 1 - \left(\frac{2}{ka}\right)^{2/3} \frac{q_p}{15} e^{j\frac{2\pi}{3}} \right\}$$

and

$$(A\text{-}30) \qquad L_p^s = e^{-j\frac{\pi}{12}} (2\pi k)^{1/2} \left(\frac{2}{ka}\right)^{2/3} Ai'(-q_p) \times \left[1 - \left(\frac{2}{ka}\right)^{2/3} \frac{1}{15} q_p e^{j\frac{2\pi}{3}} \right] D_p^s$$

where D_p^s is the soft EM diffraction coefficient given in Table I.

2. E-plane ($\phi = \frac{\pi}{2}$) Hard EM Boundary

From Eqs. (A-13) and (A-14)

$$\text{(A-31)} \qquad \overline{E} \sim \hat{\theta}\, j \frac{k^2 p_m}{4\pi} \frac{e^{-jkR}}{kR} \sqrt{\frac{\pi}{2ka}} \sum_{n=1}^{\infty} (-j)^n \frac{2n+1}{2} \left\{ H^{(1)}_{n+\frac{1}{2}}(ka) - \right.$$

$$\left. - \frac{\tilde{Q}\, H^{(1)}_{n+\frac{1}{2}}(ka)}{\tilde{Q}\, H^{(2)}_{n+\frac{1}{2}}(ka)} H^{(2)}_{n+\frac{1}{2}}(ka) \right\} \frac{dP_n^{-1}}{d\theta}(-\cos\theta)$$

Eq. (A-31) resembles Eq. (A-15) and we proceed in the same manner to a form which can be compared with the GTD solution. Employing the Watson transformation and the Cauchy residue theorem as in the preceding case

$$\text{(A-32)} \qquad E_\theta \sim j \frac{kp_m}{2} \frac{e^{-jkR}}{R} \sqrt{\frac{\pi}{2ka}} \sum_{p=1}^{\infty} \frac{e^{-j\nu_p \frac{\pi}{2}} e^{-j\frac{\pi}{4}}}{1 + e^{-j2\nu_p \pi}} \nu_p \times$$

$$\times \frac{\tilde{Q}\, H^{(1)}_{\nu_p}(ka)}{\frac{\partial}{\partial \nu} \tilde{Q}\, H^{(2)}_{\nu_p}(ka)} H^{(2)}_{\nu_p}(ka) \frac{\partial}{\partial \theta} P^{-1}_{\nu_p - \frac{1}{2}}(-\cos\theta)$$

in which ν_p are the complex orders for which

$$\tilde{Q}\, H^{(2)}_{\nu_p}(ka) = 0.$$

$$\text{(A-33)} \qquad \nu_p = ka + \left(\frac{ka}{2}\right)^{1/3} \overline{q}_p\, e^{-j\frac{\pi}{3}}$$

to first order. $\overline{q}_p$ is real and defined by the above two equations.

From Eqs. (A-18) and (A-21), where $_p$ in Eq. (A-18) has been replaced by its approximation given by (A-33)

$$(A\text{-}34) \qquad E_\theta \sim -\frac{jk}{4\pi}\frac{p_m}{\sin\theta}\sum_{p=1}^{\infty}\left\{-\pi\left(\frac{jk}{2\pi}\right)^{1/2} H_{\nu_p}^{(2)}(ka)D_p^h\right\}$$

$$\times\left[e^{-j\nu_p\psi_1} + j\,e^{-j\nu_p\psi_2}\right] D_p^h\,\frac{e^{-jkR}}{R}$$

which is the asymptotic approximation for the electric field in the shadow region of the E-plane for $\theta < \pi$. The D_p^h is the hard EM diffraction coefficient given in Table I.

The corresponding GTD solution is derived in the same manner as in the preceding section, except that $\bar{p}_m \cdot \hat{t}' = 0$ and $\bar{p}_m \cdot \hat{b} = p_m$ here, so that we begin with Eq. (12). The GTD expression for the electric field in the shadow region of the E-plane is

$$(A\text{-}35) \qquad E_\theta = \frac{Cp_m}{\sqrt{\sin\theta}}\sum_{p=1}^{\infty} L_p^h\, D_p^h\left[e^{-(jk+\alpha_p^h)a\psi_1} + je^{-(jk+\alpha_p^h)a\psi_2}\right]\frac{e^{-jkR}}{R} \quad ;$$

Comparing it with Eq. (A-34),

$$(A\text{-}36) \qquad C = -\frac{jk}{4\pi},$$

$$(A\text{-}37) \qquad L_p^h = -j\pi\left(\frac{jk}{2\pi}\right)^{1/2} H_{\nu_p}^{(2)}(ka)D_p^h,$$

$$\nu_p = ka - j\alpha_p^h a.$$

The formula for α_p^h like that of α_p^s, has been obtained previously, see Table I. Asymptotically approximating $H_\nu^{(2)}(ka)$ in terms of an Airy function

$$(A\text{-}38) \qquad H_\nu^{(2)}(ka) \sim 2\,e^{j\frac{\pi}{3}}\left(\frac{2}{ka}\right)^{1/3} Ai(-\bar{q}_p)\left\{1 + \left(\frac{2}{ka}\right)^{2/3} e^{j\frac{2\pi}{3}}\right\}$$

and

$$(A\text{-}39) \qquad L_p^h = e^{j\frac{\pi}{12}} (2\pi k)^{1/2} \left(\frac{2}{ka}\right)^{1/3} Ai(-\bar{q}_p) \times$$

$$\left[1 + \left(\frac{2}{ka}\right)^{2/3} \frac{1}{15\bar{q}_p} e^{j\frac{2\pi}{3}}\right] D_p^h.$$

where D_p^h is the hard EM diffraction coefficient given in Table I.

The desired launching coefficients are given by Eqs. (A-30) and (A-39), but before we can extend these results to more general convex surfaces, it must be determined to what extent they depend on the spherical surface employed in the canonical problem. To answer this question the radiation from magnetic line sources on a cylinder will be treated next.

3. Cylindrical surfaces

In the two-dimensional source free region exterior to the closed contour L, which is the cross section of the cylinder here, the scalar field

$$(A\text{-}40) \qquad \psi(\bar{\rho}) = \oint_L [\psi(\bar{\rho}') \frac{\partial}{\partial n'} G(\bar{\rho}', \bar{\rho}) - G(\bar{\rho}', \bar{\rho}) \frac{\partial \psi}{\partial n'}(\rho')] d\ell'$$

in which $G(\bar{\rho}, \bar{\rho}')$ is a Green's function, dn' is an infinitesimal distance taken along the outward direction to the contour L, and the direction of integration is taken in the clockwise sense. The Green's function satisfies the partial differential equation

$$(A\text{-}41) \qquad [\nabla_t^2 + k^2] G(\bar{\rho}, \bar{\rho}') = - \delta(\bar{\rho} - \bar{\rho}'),$$

where ∇_t^2 is the two-dimensional Laplacian operator and $\bar{\rho}$ and $\bar{\rho}'$ are the position vectors for the field and source points, respectively. Eq. (A-40) will be employed to find the electric field radiated by two types of axial line sources (see Eqs. (20) and (21) on a circular cylinder).

Let a magnetic line current $\bar{M} = \hat{z} M_z$ be located at $\rho' = a$, $\phi' = 0$ on the surface of a perfectly-conducting circular cylinder of radius a. On the surface of the cylinder $E_\phi(a, \phi') = M_z \delta(\phi')/a$. If

$$(A\text{-}42) \qquad H_z(\bar{\rho}) = \psi(\bar{\rho})$$

and

$$\text{(A-43)} \qquad \frac{\partial}{\partial \rho'} G_h(\bar{\rho}', \bar{\rho}) = 0 \text{ for } \rho' = a,$$

$$\text{(A-44)} \qquad H_z(\bar{\rho}) = -\oint_L G_h(\bar{\rho}, \bar{\rho}') \frac{\partial H_z(\bar{\rho}')}{\partial \rho'} \, d\ell'.$$

Since

$$\text{(A-45)} \qquad \frac{\partial H_z}{\partial \rho'} = - j\omega\varepsilon E_\phi = - j\omega\varepsilon M_z \, \delta(\phi')/a \, ,$$

$$\text{(A-46)} \qquad E_\phi(\bar{\rho}) = M_z \frac{\partial}{\partial \rho} G_h(\bar{\rho}, \hat{x}a).$$

Next let a magnetic line source $\bar{M} = -\hat{\phi}' M_\phi$ be located at $\rho' = a$, $\phi' = 0$ on the surface of a perfectly-conducting surface of radius a. On the surface of the cylinder $E_z(a,\phi') = - M_\phi \, \delta(\phi')/a$. If $E_z(\bar{\rho}) = \psi(\bar{\rho})$ in this case and

$$\text{(A-47)} \qquad G_s(a\hat{\rho}', \bar{\rho}) = 0,$$

$$\text{(A-48)} \qquad E_z(\bar{\rho}) = \oint_L E_z(\bar{\rho}') \frac{\partial}{\partial \rho'} G_s(\bar{\rho}', \bar{\rho}) \, d\ell',$$

$$E_z(\bar{\rho}) = + M_\phi \frac{\partial}{\partial \rho'} G_s(\bar{\rho}', \bar{\rho}) \Big|_{\bar{\rho}' = a\hat{x}} .$$

The Green's functions G_h, G_s which satisfy Eq. (A-41), the boundary conditions in Eqs. (A-43) and (A-47), and the radiation condition are

$$\text{(A-49)} \qquad G(\rho,\phi;\, a,\, 0) = - \frac{j}{4} \sum_{m=0}^{\infty} \varepsilon_m \left[J_m(ka) - \frac{Q\, J_m(ka)}{Q\, H_m^{(2)}(ka)} H_m^{(2)}(ka) \right] H_m^{(2)}(k\rho) \cos m\phi$$

in which $Q = \frac{d}{d\rho}$ for G_h and 1 for G_s, and

$$\varepsilon_m = \begin{cases} 1, & m = 0 \\ 2, & m \neq 0 \end{cases} .$$

Employing the Watson transformation and computing the residues of the integrand again, we transform Eq. (A-49) to a form suitable for an asymptotic approximation and ray optical interpretation.

$$(A\text{-}50)\qquad G(\rho,\phi;\, a,\, 0) =$$

$$\frac{\pi}{4j}\sum_{p=0}^{\infty}\frac{Q\,H^{(1)}_{\nu_p}(ka)}{\left[\frac{\partial}{\partial\nu}Q\,H^{(2)}(ka)\right]_{\nu=\nu_p}}\,H^{(2)}_{\nu_p}(ka)H^{(2)}_{\nu_p}(k\rho)\left[e^{-j\nu_p\psi_1}+e^{-j\nu_p\psi_2}\right]e^{-j\nu_p\frac{\pi}{2}}$$

with ν_p the zeroes of $Q\,H^{(2)}_{\nu_p}(ka) = 0$. We have used

$$(A\text{-}51)\qquad \frac{\cos\nu_p\phi}{\sin\nu_p} = \frac{e^{-j\nu_p\psi_1}+e^{-j\nu_p\psi_2}}{1-e^{-j2\pi\nu_p}}\,e^{-j\nu_p\frac{\pi}{2}},$$

$$(A\text{-}52a,b)\qquad \psi_1 = \phi - \frac{\pi}{2},\qquad \psi_2 = \frac{3\pi}{2} - \phi$$

and approximated $(1 - e^{-j2\pi\nu_p})^{-1}$ by 1 for ka large.

Introducing the definition of the diffraction coefficient

$$(A\text{-}53)\qquad \frac{Q\,H^{(1)}_{\nu_p}(ka)}{\frac{\partial}{\partial\nu}Q\,H^{(2)}_{\nu_p}(ka)} = -\left(\frac{jk}{2\pi}\right)^{1/2}\left[D_{op}\right]^2$$

in which $Q = \frac{\partial}{\partial\rho}$ for D^h_{op} and 1 for D^s_{op}, and the asymptotic approximation

$$(A\text{-}54)\qquad H^{(2)}_{\nu}(k\rho) \sim \sqrt{\frac{2}{\pi k\rho}}\,e^{-j[k\rho-(2\nu+1)\frac{\pi}{4}]},$$

the electric fields given by Eqs. (A-46) and (A-48) may be determined in the far-zone for ka large. For the circular cylinder $D_{op} = D_p$. Thus

$$(A\text{-}55)\qquad E_\phi = \frac{-jkM_z}{\sqrt{8\pi kj}}\sum_{p=1}^{\infty}\left[-j\pi\left(\frac{jk}{2\pi}\right)^{1/2}H^{(2)}_{\nu_p}(ka)\,D^h_p\right]x$$
$$x\left[e^{-j\nu_p\psi_1}+e^{-j\nu_p\psi_2}\right]D^h_p\,\frac{e^{-jk\rho}}{\sqrt{\rho}}$$

and

$$(A\text{-}56) \qquad E_z = \frac{-jkM}{\sqrt{8\pi kj}} \sum_{p=1}^{\infty} [-\pi(\frac{jk}{2\pi})^{1/2} H_{\nu_p}^{(2)'}(ka)\, D_p^s] \times$$

$$\times [e^{-j\nu_p\psi_1} + e^{-j\nu_p\psi_2}]\, D_p^s \frac{e^{-jk\rho}}{\sqrt{\rho}} .$$

Note that $\frac{\partial}{\partial\rho'} G_s(\bar{\rho}', \bar{\rho})$ may be obtained from Eq. (A-50) by replacing $H_{\nu_p}^{(2)}(ka)$ in the numerator by its derivative with respect to ρ, $kH_{\nu_p}^{(2)'}(ka)$.

Referring to Fig. 2A, the corresponding GTD expressions for E_ϕ and E_z are readily deduced from Eqs. (12), (14), (22) and (24) in the manner described in the appendix. Thus

$$(A\text{-}57) \qquad E_\phi = C\, M_z \sum_{p=1}^{\infty} L_p^h D_p^h [e^{-(jk+\alpha_p^h)a\psi_1} + e^{-(jk+\alpha_p^h)a\psi_2}] \frac{e^{-jk\rho}}{\sqrt{\rho}}$$

and

$$(A\text{-}58) \qquad E_z = C\, M_\phi \sum_{p=1}^{\infty} L_p^s D_p^s [e^{-(jk+\alpha_p^s)a\psi_1} + e^{-(jk+\alpha_p^s)a\psi_2}] \frac{e^{-jk\rho}}{\sqrt{\rho}} .$$

Comparing Eqs. (A-57), (A-58) with Eqs. (A-55), (A-56), respectively, it is seen that

$$(A\text{-}59) \qquad C = -\frac{k\, e^{j\frac{\pi}{4}}}{\sqrt{8\pi k}} ,$$

$$(A\text{-}60) \qquad L_p^h = -j\pi(\frac{jk}{2\pi})^{1/2} H_{\nu_p}^{(2)}(ka)\, D_p^h ,$$

$$(A\text{-}61) \qquad L_p^s = -\pi\,(\frac{jk}{2\pi})^{1/2} H_{\nu_p}^{(2)'}(ka)\, D_p^s .$$

It is found that the second order asymptotic approximations of $H_{\nu_p}^{(2)}(ka)$ and $H_{\nu_p}^{(2)'}(ka)$ are given by Eqs. (A-38) and (A-29), which is interesting because the ν_p are different to order $(2/ka)^{4/3}$ in the solutions to the hard sphere and hard cylinder problems. Using these asymptotic approximations together with the cylinder diffraction coefficients listed in Table I, one can obtain the hard and soft launching coefficients for the cylinder to second order.

Comparing Eq. (A-60) with Eq. (A-37) and Eq. (A-61) with Eq. (A-27) and noting the asymptotic behavior of the Hankel function and its derivative just mentioned, leads us to conjecture that in the case of a general convex surface the launching coefficients are given by Eqs. (35) and (36) in the text.

APPENDIX II
THE FIELD IN THE TRANSITION REGION

In the transition region adjacent to the shadow boundary, the representation of the field radiated by the slots described in Appendix I is poorly convergent, so a different form is needed. It will be seen that a suitable asymptotic solution can be obtained in terms of integrals. The first order approximation is usually adequate for ka>3, and since the added complexity of the second order approximation is difficult to justify, we will derive only the first order approximation. Furthermore, since the first order approximations for the cylinder and the sphere are the same, except for a factor $d\psi_0/d\psi$ which is present in the latter case, only the cylinder problem will be treated here.

The Watson transformation is applied to Eq. (A-49) again, but this time the resulting expression is left in the form of an integral. In the far-zone $H_\nu^{(2)}(k\rho)$ is approximated asymptotically as in Eq. (A-54) so that

(A-62)

$$G_h(P|Q') \sim -\frac{1}{2\sqrt{8\pi kj}}\frac{e^{-jk\rho}}{\sqrt{\rho}}\sum_{\ell=0}^{\infty}\int_{-\infty}^{\infty}d\nu\left\{\frac{H_\nu^{(1)}(ka)H_\nu^{(2)'}(ka)-H_\nu^{(2)}(ka)H_\nu^{(1)'}(ka)}{H_\nu^{(2)'}(ka)}\right\}$$

$$\left[e^{-j\nu(\psi_1+2\pi\ell)}+e^{-j\nu(\psi_2+2\pi\ell)}\right]$$

(A-63)

$$\frac{\partial G_s(P|Q')}{\partial\rho'} \sim -\frac{K}{2\sqrt{8\pi kj}}\frac{e^{-jk\rho}}{\sqrt{\rho}}\sum_{\ell=0}^{\infty}\int_{-\infty}^{\infty}d\nu\left\{\frac{H_\nu^{(1)'}(ka)H_\nu^{(2)}(ka)-H_\nu^{(2)'}(ka)H_\nu^{(1)}(ka)}{H_\nu^{(2)}(ka)}\right\}$$

$$\left[e^{-j\nu(\psi_1+2\pi\ell)}+e^{-j\nu(\psi_2+2\pi\ell)}\right]$$

where $\psi_1 = \phi - \pi/2$, and $\psi_2 = \frac{3\pi}{2} - \phi$, as in Appendix I.

From the Wronskian relationship for the two types of Hankel functions,

$$(A\text{-}64)\quad H_\nu^{(1)'}(ka)\,H_\nu^{(2)}(ka) - H_\nu^{(2)'}(ka)\,H_\nu^{(1)}(ka) = \frac{4j}{\pi ka}\ .$$

Using Eq. (A-64) in Eqs. (A-62) and (A-63)

$$(A\text{-}65)\quad G_h(P/Q') \sim \frac{2j}{\pi ka}\,\frac{1}{\sqrt{8\pi kj}}\,\frac{e^{-jk\rho}}{\sqrt{\rho}} \sum_{\ell=0}^{\infty} \int_{-\infty}^{\infty} d\nu \left[\frac{e^{-j\nu(\psi_1+2\pi\ell)} + e^{-j\nu(\psi_2+2\pi\ell)}}{H_\nu^{(2)'}(ka)}\right]$$

and

$$(A\text{-}66)\quad \frac{\partial G_s(P/Q')}{\partial \rho'} \sim -\frac{2jk}{\pi ka}\,\frac{1}{\sqrt{8\pi kj}}\,\frac{e^{-jk\rho}}{\sqrt{\rho}} \sum_{\ell=0}^{\infty} \int_{-\infty}^{\infty} d\nu \left[\frac{e^{-j\nu(\psi_1+2\pi\ell)} + e^{-j\nu(\psi_2+2\pi\ell)}}{H_\nu^{(2)}(ka)}\right].$$

Replacing $H_\nu^{(2)}(ka)$ and $H_\nu^{(2)'}(ka)$ in (A-65) and (A-66) by their Watson approximations (for $\nu \approx ka \gg 1$) gives rise to the Fock function representations for G_h and $\partial G_s/\partial \rho'$.

$$(A\text{-}67)\quad G_h(P/Q') \sim \frac{2j}{\pi ka}\,\frac{-jk}{(8\pi kj)^{1/2}}\,\frac{1}{-jk} \sum_{\ell=0}^{\infty} \left[e^{-jka(\psi_1+2\pi\ell)}\,\frac{ka}{2}\,j\sqrt{\pi}\int_{\Gamma_1} \frac{e^{-j\xi_1\tau}}{w_2'(\tau)}\,d\tau + \right.$$

$$\left. + e^{-jka(\psi_2+2\pi\ell)}\,\frac{ka}{2}\,j\sqrt{\pi}\int_{\Gamma_1} \frac{e^{-j\xi_2\tau}}{w_2'(\tau)}\,d\tau\right] \frac{e^{-jk\rho}}{\sqrt{\rho}}$$

and

(A-68)

$$\frac{\partial G_s(P/Q')}{\partial \rho'} \sim \frac{2}{\pi ka}\left\{\frac{-jk}{(8\pi kj)^{1/2}}\right\} \sum_{\ell=0}^{\infty} \left[e^{-jka(\psi_1+2\pi\ell)}\left(\frac{ka}{2}\right)^{2/3}(-j\sqrt{\pi})\int_{\Gamma_1} \frac{e^{-j\xi_1\tau}}{w_2(\tau)}\,d\tau + \right.$$

$$\left. + e^{-jka(\psi_2+2\pi\ell)}\left(\frac{ka}{2}\right)^{2/3}(-j\sqrt{\pi})\int_{\Gamma_1} \frac{e^{-j\xi_2\tau}}{w_2(\tau)}\,d\tau\right] \frac{e^{-jk\rho}}{\sqrt{\rho}}$$

with

$$H_\nu^{(2)}(ka) \sim \frac{j}{\sqrt{\pi}} \left(\frac{2}{ka}\right)^{1/3} w_2(\tau), \tag{A-69}$$

$$H_\nu^{(2)'}(ka) \sim \frac{-j}{\sqrt{\pi}} \left(\frac{2}{ka}\right)^{2/3} w_2'(\tau), \tag{A-70}$$

and

$$\xi_{\frac{1}{2}} = \left(\frac{ka}{2}\right)^{1/3} \psi_{\frac{1}{2}}. \tag{A-71}$$

Here $w_2(\tau)$ is a Fock-type Airy function related to the Miller-type Airy function by

$$W_2(\tau) = 2\sqrt{\pi}\, e^{-j\frac{\pi}{6}} Ai(-\tau e^{j\frac{\pi}{3}}); \tag{A-72a}$$

alternatively, it may be defined by

$$W_2(\tau) = \frac{1}{\sqrt{\pi}} \int_{\Gamma_2} e^{\tau z - z^3/3}\, dz \tag{A-72b}$$

$$W_2'(\tau) = \frac{1}{\sqrt{\pi}} \int_{\Gamma_2} z\, e^{\tau z - z^3/3}\, dz \tag{A-72c}$$

with the contour of integration Γ_2 shown in Fig. 3A.

Introducing the Fock functions

$$g(\xi) = \frac{1}{\sqrt{\pi}} \int_{\Gamma_1} \frac{e^{-j\xi\tau}}{w_2'(\tau)}\, d\tau \tag{A-73}$$

and

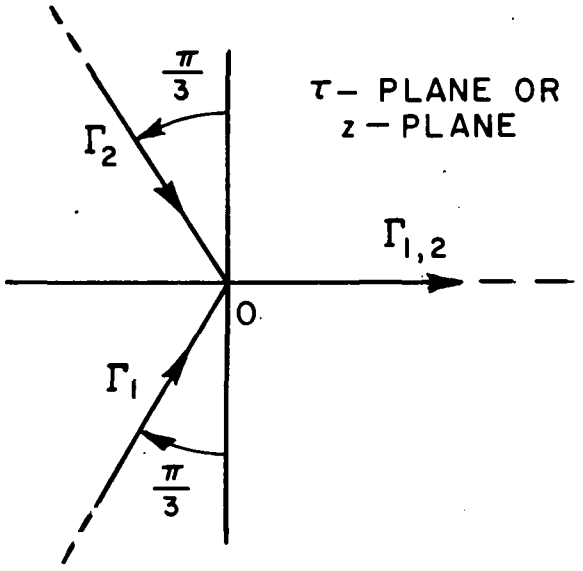

Fig. 3A. Contours of integration for the Airy and Fock functions.

$$(A\text{-}74) \qquad \tilde{g}(\xi) = \frac{1}{\sqrt{\pi}} \int_{\Gamma_1} \frac{e^{-j\xi\tau}}{w_2(\tau)}\, d\tau,$$

$$(A\text{-}75) \qquad G_h(P/Q') \sim -j\,\frac{C}{k}\left\{g(\xi_1)\, e^{-jka\psi_1} + g(\xi_2)\, e^{-jka\psi_2}\right\}\frac{e^{-jk\rho}}{\sqrt{\rho}}$$

and

$$(A\text{-}76) \qquad \frac{\partial G_s(P/Q')}{\partial \rho'} \sim -j\, C\, \left(\frac{2}{ka}\right)^{1/3}\left\{\tilde{g}(\xi_1)e^{-jka\psi_1} + \tilde{g}(\xi_2)e^{-jka\psi_2}\right\}\frac{e^{-jk\rho}}{\sqrt{\rho}}$$

where

$$C \equiv -jk(8\pi kj)^{-1/2},$$

and only the first term $\ell=0$ is retained for large ka. When the Fock functions are represented by a residue series [16], it is seen that they become negligible for $\xi>>1$, which justifies ignoring the higher order terms in the series.

Substituting the preceding expressions into Eqs. (A-46) and (A-48) the far-zone electric fields for the line sources $\hat{z}\, M_z$ and $\hat{\phi}\, M_\phi$ are

$$(A\text{-}77) \qquad E_\phi \sim C\, M_z \left[g(\xi_1) e^{-jka\psi_1} + g(\xi_2) e^{-jka\psi_2} \right] \frac{e^{-jk\rho}}{\sqrt{\rho}}$$

and

$$(A\text{-}78) \qquad E_z \sim C\, M_\phi \left\{ -j\left(\frac{2}{ka}\right)^{1/3} \right\} \left[\tilde{g}(\xi_1) e^{-jka\psi_1} + \tilde{g}(\xi_2) e^{-jka\psi_2} \right] \frac{e^{-jk\rho}}{\sqrt{\rho}} \quad .$$

The above asymptotic representations of E_ϕ and E_z may be interpreted ray optically, as in the preceding appendix. Referring to Fig. II-A, the first term in each equation is the field of ray 1, and the second term is the field of ray 2. In the transition region $\psi_1 = \phi - \pi/2$ is of order $(ka)^{-1/3}$, and for large ka assumed here, this angle is small; on the other hand, $\psi_2 \approx \pi$. Ray 1 traverses only a short distance $\psi_1 a$ on the surface before radiating. The field contribution from ray 2 is more accurately represented by the expressions of Appendix I, since they are accurate to order 2, and this accuracy is important if the ray has traversed a substantial distance on the surface between its source and the point of radiation Q_2. However, it is the representation of the field of ray 1 which is of interest here, so we will not include the contribution from ray 2 in the discussion to follow.

Comparing Eqs. (A-77) and (A-78) with Eqs. (A-57) and (A-58) and with Eq. (24) it is seen that

$$(A\text{-}79) \qquad F = g(\xi_1) e^{-jka\psi_1}$$

and

$$(A\text{-}80) \qquad G = -\, j\left(\frac{2}{ka}\right)^{1/3} g(\xi_1)\, e^{-jka\psi_1} .$$

These integral representations of F and G may be used in place of the poorly convergent series of surface ray modes in the transition region. However, the series representations of F and G useful in the shadow region can be obtained directly from their integral representations, showing that the two solutions join smoothly to first order. This will be discussed next.

In the deep shadow ξ is large and positive and the Fock integrals may be replaced by a residue series[16], so that

$$(A\text{-}81) \qquad F = \sum_{p=1} \frac{e^{\xi \bar{q}_p e^{j\frac{5\pi}{6}}} e^{-jka\psi_1}}{\bar{q}_p Ai(-\bar{q}_p)}$$

$$(A\text{-}82) \qquad G = -j\left(\frac{2}{ka}\right)^{1/3} e^{j\frac{\pi}{3}} \sum_{p=1} \frac{e^{\xi q_p e^{-j\frac{5\pi}{6}}} e^{-jka\psi_1}}{Ai'(-q_p)}$$

which equal

$$(A\text{-}83) \qquad F = \sum_p L_p^h D_p^h e^{-(jk+\alpha_p^h)a\psi_1},$$

$$(A\text{-}84) \qquad G = \sum_p L_p^s D_p^s e^{-(jk+\alpha_p^s)a\psi_1},$$

when the first order approximations for the diffraction coefficients and attenuation constants, see Eqs. (26) through (28), and the first order approximations for the launching coefficients

$$(A\text{-}85) \qquad L_{op}^s = e^{-j\frac{\pi}{12}} (2\pi k)^{1/2} \left(\frac{2}{ka}\right)^{2/3} Ai'(-q_p) D_{op}^s$$

$$(A\text{-}86) \qquad L_{op}^h = e^{j\frac{\pi}{12}} (2\pi k)^{1/2} \left(\frac{2}{ka}\right)^{1/3} Ai(-\bar{q}_p) D_{op}^h$$

are employed. The two equations above follow from Eqs. (A-27) and (A-39).

It is also important that the integral representations of the field in the transition region join smoothly with the geometrical optics field, given by Eqs. (18) and (24), in the illuminated region. Deep in the illuminated region ξ is large and negative with the result that the Fock functions may be approximated asymptotically[16].

(A-87) $$g(\xi) \sim 2\, e^{j\xi^3/3}$$

(A-88) $$\tilde{g}(\xi) \sim -2j\xi e^{j\xi^3/3} .$$

Substituting the above expressions into Eqs. (A-79) and (A-80)

(A-89) $$F \sim 2\, e^{-jka\sin\psi_1}$$

(A-90) $$G \sim -2\,\psi_1\, e^{-jka\sin\psi_1}$$

in which we have employed $\psi_1 - \psi_1^3/6 \simeq \sin\psi_1$.

Equation (A-89) is recognized as the geometrical optics form of F, when one notes that the exponential term gives the phase delay between the point of radiation Q_1 and the source located at Q', see Fig. 4A. As pointed out in Chapter III, in the illuminated part of the transition region, one visualizes the surface ray as traveling from the source at Q' to the point of radiation at Q_1 where it sheds a ray tangentially toward P as indicated in Figs. 7 and 4A. The representation of F given in Eq. (A-79) may be used in both the illuminated and transition regions.

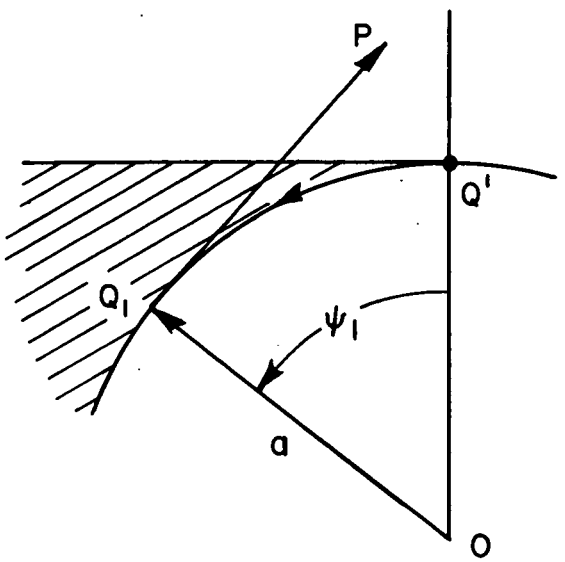

Fig. 4A. An equivalent ray system for calculating the radiation in the illuminated region.

On the other hand, the asymptotic form of G in Eq. (A-90) does not join smoothly with the geometrical optics solution,

$$G \sim -2 \sin\psi_1 e^{-jka\sin\psi_1}, \tag{A-91}$$

unless one modifies Eq. (A-80) in the following way

$$G = -j\left(\frac{2}{ka}\right)^{1/3} \tilde{g}(\xi_1) f(\psi_1) e^{jka\psi_1} \tag{A-92}$$

with

$$f(\psi_1) = \begin{cases} \dfrac{\sin\psi_1}{\psi_1}, & -\dfrac{\pi}{2} < \psi_1 \leq 0 \\ 1, & \psi_1 \geq 0 \end{cases} . \tag{A-93}$$

Equation (A-92) has been justified through its application to numerous examples; it should be regarded as an algorithm for calculating G in the transition region so that it joins smoothly with the geometrical optics field, which is valid deep in the illuminated region.

APPENDIX III
DERIVATION OF THE FIELDS AT AN AXIAL CAUSTIC OF THE DIFFRACTED RAYS

Consider a perfectly-conducting convex surface of revolution with an infinitesimal slot positioned on its axis of revolution at Q' as shown in Fig. 5A. There is a caustic of the diffracted rays on the axis of revolution in the shadow region and the ordinary GTD solution breaks down here. This appendix describes how the GTD solution may be supplemented by an integral representation of the field to obtain a high frequency approximation at the axial caustic. However, it will be seen that the GTD is used to deduce the equivalent sources of the integral representation. The field in the shadow region (excluding the negative z axis) is obtained by a superposition of the fields associated with the rays shed from only two points Q_1 and Q_2 on the surface of revolution, as shown in Fig. A2. In the vicinity of the caustic (z-axis), the rays arriving at P are shed from a continuum of points constituting a ring of radius 'a' on the surface as shown in Fig. 5A; the radial distance 'a' is the maximum perpendicular distance from the z-axis to the surface.

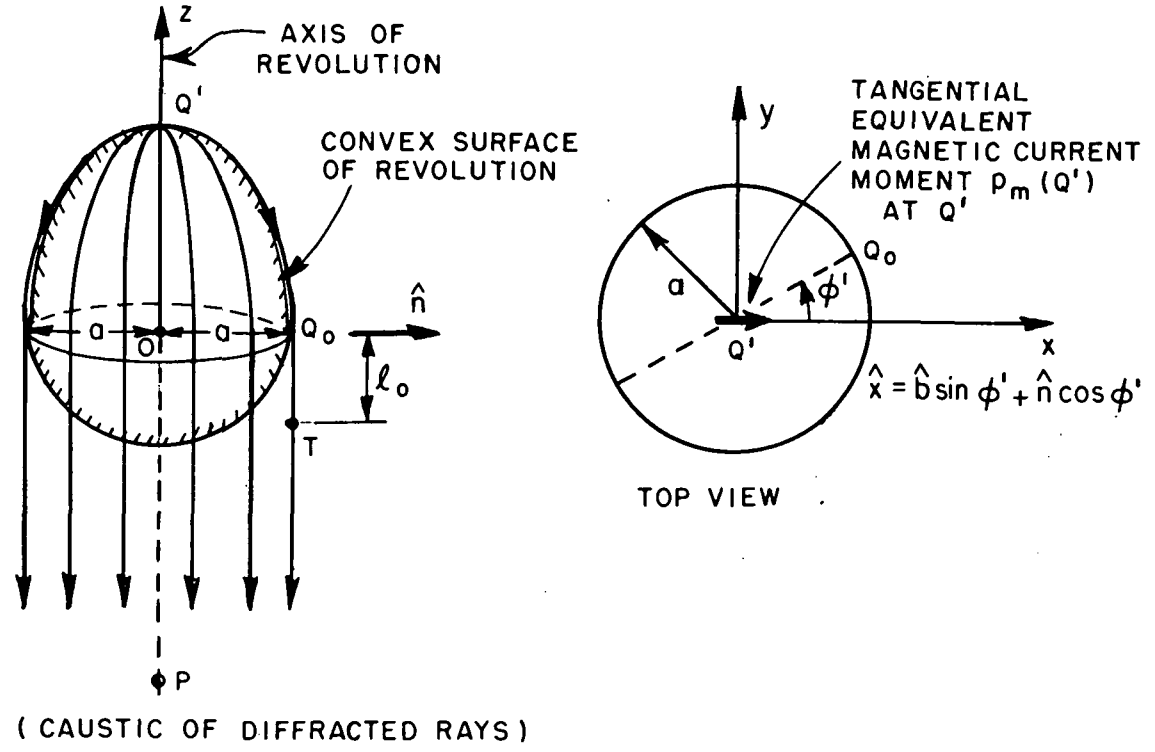

Fig. 5A. Ray geometry for calculating the field at an axial caustic.

The equivalent source for the infinitesimal slot at Q' is a magnetic current moment of strength $p_m\hat{x}$ at Q' which is oriented along the slot axis as shown in Fig. 5-A. This equivalent source produces an electric field at the point, T located at $\rho=a$, $\phi=\phi'$, $z=-\ell_o$. This point is in the near zone of the surface of revolution, but it is several wavelengths from Q_o, the point at which the surface ray sheds toward T. The GTD result for the electric field at T is

$$\text{(A-94)} \qquad \overline{E}(T) = C\, p_m \{\hat{n}\sin\phi' F_o + \hat{b}\cos\phi' G_o\} \sqrt{\frac{d\psi_o}{d\eta}} \sqrt{\frac{\rho}{\ell_o(\rho+\ell_o)}}\, e^{-jk\ell_o},$$

where

$$\text{(A-95)} \qquad F_o = \sum_{p=1}^{\infty} L_p^h(Q') D_p^h(Q_o)\, e^{-jk\int_{Q'}^{Q_o} dt'}\, e^{-\int_{Q'}^{Q_o} \alpha_p^h(t')dt'},$$

$$\text{(A-96)} \qquad G_o = \sum_{p=1}^{\infty} L_p^s(Q') D_p^s(Q_o)\, e^{-jk\int_{Q'}^{Q_o} dt'}\, e^{-\int_{Q'}^{Q_o} \alpha_p^s(t')dt'},$$

$$C = -jk/4\pi \ ,$$

and the quantity $d\eta$, and the caustic distance, ρ are defined in Chapter II. Note that F_o and G_o are the same as the F and G functions without the factor $\sqrt{d\psi_o/d\psi}$. For the ray shed in the caustic direction, $\rho\to\infty$, so that Eq. (A-94) becomes

$$\text{(A-97)} \qquad \overline{E}(T) \approx [C\, p_m \{\hat{n}\sin\phi' F_o + \hat{b}\cos\phi' G_o\} \frac{1}{\sqrt{a}}] \cdot \frac{e^{-jk\ell_o}}{\sqrt{\ell_o}} \ .$$

The integral representations for the electric fields at T radiated by electric and magnetic ring currents of strengths $I_o(\phi")$, and $M_o(\phi")$, respectively are

$$\text{(A-98)} \qquad \overline{E}_e(T) \approx \frac{jka}{4\pi}\int_0^{2\pi} [Z_o(\hat{r}x\hat{r}xI_o(\phi")\hat{\phi}")] \frac{e^{-jkr}}{r}\, d\phi",$$

and

$$\text{(A-99)} \qquad \overline{E}_m(T) \approx \frac{jka}{4\pi} \int_0^{2\pi} [\hat{r} x M_o(\phi'')\hat{\phi}''] \frac{e^{-jkr}}{r} \, d\phi'' \,,$$

where

$$Z_o = Y_o^{-1} = \sqrt{\mu_o/\varepsilon_o},$$

a is the radius of the ring currents,

$$r = \sqrt{\ell_o^2 + 2a^2[1-\cos(\phi'-\phi'')]},$$

and the subscripts e and m refer to the electric field contributions from the electric type and magnetic type ring currents, respectively. The unit vector r is directed from ϕ'' on the ring to T. If one evaluates the above integrals by the method of stationary phase, one finds that there is a stationary phase point at Q_o. The contributions to the field at T which arise from this stationary point are

$$\text{(A-100)} \qquad \overline{E}_e(T) \sim -\hat{b}\, k\, Z_o \frac{e^{j\frac{\pi}{4}}}{\sqrt{8\pi k}} I_o(\phi') \frac{e^{-jk\ell_o}}{\sqrt{\ell_o}} \,,$$

and

$$\text{(A-101)} \qquad \overline{E}_m(T) \sim -\hat{n}\, k \frac{e^{j\frac{\pi}{4}}}{\sqrt{8\pi k}} M_o(\phi') \frac{e^{-jk\ell_o}}{\sqrt{\ell_o}} \,.$$

A comparison of Eq. (A-97) with Eq. (A-100) and Eq. (A-101) indicates that the GTD field at T may be considered to have the equivalent electric and magnetic ring currents whose strengths $I_o(\phi')$ and $M_o(\phi')$ respectively are given by

$$\text{(A-102)} \qquad I_o(\phi') = -C\, p_m\, Y_o \cos\phi'\, G_o\, e^{-j\frac{\pi}{4}} \left(\frac{8\pi}{ka}\right)^{1/2} \,,$$

and

$$(A\text{-}103) \quad M_o(\phi') = - C\, p_m \sin\phi'\, F_o\, e^{-j\frac{\pi}{4}} \left(\frac{8\pi}{ka}\right)^{1/2} .$$

The radiation field in the vicinity of the caustic is therefore the field radiated by these equivalent ring currents. This technique of using equivalent currents based on the GTD to describe the fields in the vicinity of the axial caustic of the diffracted rays has been used with success elsewhere in problems involving curved edge diffraction[17,18]; however, unlike the curved edge, the rim indicated in Fig. 5A does not stay fixed as the observation point moves slightly away from the caustic, and hence the caustic solution presented here is not expected to be accurate at aspects not close to the axial caustic. The expression for the far-zone electric field due to the $\hat{\phi}'$ directed electric and magnetic ring current sources of strengths $I_o(\phi')$ and $M_o(\phi')$ given by Eqs. (A-102) and (A-103), respectively is expressed in terms of the radiation integral as

(A-104)

$$\overline{E}(P) \approx \frac{jka}{4\pi} \frac{e^{-jks}}{s} \int_0^{2\pi} [Z_o(\hat{r}x\hat{r}xI_o(\phi')\hat{\phi}')+(\hat{r}xM_o(\phi')\hat{\phi}')]e^{jkasin\theta cos(\phi-\phi')} d\phi' .$$

This expression for $\overline{E}(P)$ in Eq. (A-104) is a general result, and the integrals involved can be evaluated in closed form; however only the integrations for the patterns in the X-Z and the Y-Z planes are needed, see the discussion connected with Eq. (60) of the text.

X-Z plane (ϕ=0)

(A-105)

$$E_{\parallel}(P) \sim + \frac{jk}{4\pi}\, p_m \left(\frac{j\pi ka}{2}\right)^{1/2} [G_o\{J_o(kasin\theta)-J_2(kasin\theta)\}+F_o cos\theta\{J_o(kasin\theta) + J_2(kasin\theta)\}] \frac{e^{-jks}}{s} .$$

Y-Z plane ($\phi=\frac{\pi}{2}$)

(A-106)

$$E_{\perp}(P) \sim + \frac{jk}{4\pi} p_m \left(\frac{j\pi ka}{2}\right)^{1/2} [G_0 \cos\theta\{J_0(ka\sin\theta)+J_2(ka\sin\theta)\}+F_0\{J_0(ka\sin\theta) - J_2(ka\sin\theta)\}] \frac{e^{-jks}}{s}$$

in which F_0, G_0 are given by Eqs. (A-95), (A-96). The $J_0(x)$ and $J_2(x)$ in Eq. (A-105) and Eq. (A-106) are cylindrical Bessel functions of the first kind with argument $x(=ka\sin\theta)$; the subscripts indicate the orders of these functions.

As mentioned before, the above results are valid only when P is in the vicinity of the axial caustic. This means that although the caustic correction is needed for the angular range $\pi - (ka)^{-1/3} < \theta \leq \pi$, the above formulas may be satisfactory only for a smaller angular range adjacent to π. This is particularly true when ka is small. Work is currently under way to improve these formulas so that they are adequate throughout the entire range $\pi - (ka)^{-1/3} < \theta \leq \pi$.

REFERENCES

1. Keller, J.B., "Geometrical Theory of Diffraction," J. Opt. Soc. Am., Vol. 52, No. 2, February 1962, pp. 116-130.

2. Sensiper, S., "Cylindrical Radio Waves," I.R.E. Trans. AP-5, pp. 56-70, 1957.

3. Wait, J.R., Electromagnetic Radiation from Cylindrical Structures, Pergamon Press, N.Y., 1959.

4. Belkina, M.G. and Weinstein, L.A., "Radiation Characteristics of Spherical Surface Antennas," in: Symposium on Diffraction of Electromagnetic Waves on Certain Bodies of Revolution, pp. 57-125, Soviet Radio, Moscow (also see Reference [16], which includes their numerical results too), 1957.

5. Goodrich, R.F., et al., "Radiation from Slot Arrays on Cones," IRE Trans., AP-7, pp. 213-222, 1959.

6. Balanis, C.A. and Peters, L., Jr., "Analysis of Aperture Radiation from an Axially Slotted Circular Conducting Cylinder Using Geometrical Theory of Diffraction," IEEE Trans. on Ants. and Prop., Vol. AP-17, No. 1, January 1969, pp. 93, 97.

7. Levy, B.R. and Keller, J.B., "Diffraction by a Smooth Object," Comm. Pure and Applied Math., 12, pp. 159-209, 1959.

8. Voltmer, D.R. and Kouyoumjian, R.G., "Diffraction Coefficients and Attenuation Constants for Convex Surfaces," paper presented at the 1970 Fall Meeting of the URSI, Columbus, Ohio. (A paper on this subject is being prepared for publication.)

9. Voltmer, D.R., "Diffraction by Doubly Curved Convex Surfaces," Ph.D. Dissertation, The Ohio State University, 1970.

10. Hong, S., "Asymptotic Theory of Electromagnetic and Acoustic Diffraction by Smooth Convex Surfaces of Variable Curvature," J. Math. Phys., 8, pp. 1223-1232, 1967.

11. Abramowitz and Stegun (Eds.): Handbook of Mathematical Functions, National Bureau of Standards Publication, June 1964, p. 478.

12. King, R.W.P. and Wu, T.T., Scattering and Diffraction of Waves, Harvard Monographs in Applied Sciences, Harvard University Press, Cambridge, Mass., 1959.

13. Harrington, R.F., Time-Harmonic Electromagnetic Fields, McGraw-Hill Book Co., New York, 1961.

14. Watson, G.N., "The Diffraction of Electrical Waves by the Earth," Proceedings of the Royal Society of London, Vol. A95, 1918.

15. Keller, J.B. and Levy, B.R., "Decay Exponents and Diffraction Coefficients for Surface Waves on Surfaces of Non-Constant Curvature," I.R.E. Trans. AP-7, pp. S52-S61, 1959.

16. Bowman, J.J. Senior, T.B.A. and Uslenghi, P.L.E. (Eds.), Electromagnetic and Acoustic Scattering by Simple Shapes, North Holland Publishing Co., 1969, pp. 380-395.

17. Ratnasiri, P.A.J., Kouyoumjian, R.G. and Pathak, P.H., "The Wide Angle Side Lobes of Reflector Antennas," Report 2183-1, The Ohio State University ElectroScience Laboratory, Columbus, Ohio, 1970.

18. Burnside, W.D. and Peters, L., Jr., "Axial Radar Cross Section of Finite Cones by the Equivalent Current Concept with Higher Order Diffraction," Radio Sci., vol. 7, Oct. 1972, pp. 1943-1948.

19. Tai, C.T., Dyadic Green's Functions in Electromagnetic Theory, International Textbook Company, 1971.

20. Tyras, G., Radiation and Propagation of Electromagnetic Waves, Academic Press, New York and London, 1969.

21. Franz, W. and Klante, K., "Diffraction by Surface of Variable Curvature," IRE Trans. AP-7, 1959.

22. Logan, Nelson A., "General Research in Diffraction Theory," Vol. 2, Report LMSD-288088, Missiles and Space Division, Lockheed Aircraft Corporation, December 1959.

23. Fock, V.A., "Electromagnetic Diffraction and Propagation Problems," Pergamon Press (1965).

24. Wetzel, L., "High Frequency Current Distribution on Conducting Obstacles," Cruft Lab. Scientific Report No. 10, Harvard Univ., 1957.

25. Burnside, W.D., "Analysis of On-Aircraft Antenna Patterns," Ph. D. Dissertation, 1972, Ohio State University, Columbus, Ohio.